

**“CAD-on” interfaces - a fracture mechanics characterization**

by

Peter David Walker

DDS, Dalhousie University, 2008

A THESIS SUBMITTED IN PARTIAL FULFILLMENT OF THE  
REQUIREMENTS FOR THE DEGREE OF

MASTER OF SCIENCE

in

THE FACULTY OF GRADUATE AND POSTDOCTORAL STUDIES  
(CRANIOFACIAL SCIENCES)

THE UNIVERSITY OF BRITISH COLUMBIA

(Vancouver)

July 2017

© Peter David Walker, 2017

## **Abstract**

**Objective:** “CAD-on” crowns, consisting of CAD/CAM milled lithium disilicate (LS2) veneers glass-fused to CAD/CAM milled yttrium oxide stabilized tetragonal zirconia polycrystal (Y-TZP) framework, have shown promise in increasing veneer fracture resistance. The glass fusion technique is purported to result in stronger bonding between veneer and framework when compared to conventional veneering. The objective of this study was to apply fracture mechanics methodology to characterize the interfaces present in “CAD-on” crowns.

**Methods:** The notchless triangular prism (NTP) specimen fracture toughness ( $K_{IC}$ ) test was used to determine interfacial  $K_{IC}$ . Four groups, each consisting of 6X6X6X12mm NTP specimens (n=22), were produced from IPS Emax CAD (LS2), IPS Emax ZirCAD (Y-TZP), and IPS Emax ZirPress and crystal connect™ (CC) fusing glass. Groups I (Emax/CC/Emax), II (Zir/CC/Zir), and III (Zir/CC/Emax) utilized half-size (6X6X6X6mm) NTP specimens approximated under vibration with the connecting glass and sintered according to manufacturers’ guidelines. Group IV specimens were coated with ZirLiner and pressed with IPS Emax ingots. The specimens were tested using a computer controlled (Bluehill) Instron 4301. Results were analyzed with one-way ANOVA, Scheffé multiple means comparisons ( $\alpha=0.05$ ) and Weibull statistics. All fractured surfaces were characterized with a light microscope. Selected fractured interfaces were characterized under a scanning electron microscope.

**Results:** Groups I-III demonstrated a cohesive mode of failure. Number and size of defects appeared to correlate with the variability of  $K_{IC}$  values. There were no significant differences

between the  $K_{IC}$  values of the “CAD-on” interfaces. Interfacial  $K_{IC}$  values were limited by  $K_{IC}$  of CC. The “CAD-on”  $K_{IC}$  value was significantly greater than that of the ZirPress control.

**Conclusion:** Based on the results obtained,  $K_{IC}$  of interfaces produced during the “CAD-on” technique appear to be limited by the interfacial  $K_{IC}$  of the connecting glass and the defects produced during processing. In this study, “CAD-on” produced veneers had stronger interfacial  $K_{IC}$  than a conventionally veneered control group.

## **Lay Summary**

Zirconia and lithium disilicate are two dental restorative materials used in CAD/CAM dentistry. Lithium disilicate restorations have been shown to perform similarly to metal-based restorations with favorable translucency and biocompatibility. Unfortunately, restorative failures continue to limit the use of lithium disilicate in the posterior region. Zirconia has garnered positive attention for its flexural strength, milling capability, and its capacity to resist crack formation. However, an opaque finish and a lack of translucency limit the esthetics applications of zirconia. The development of a new technique called “CAD-on” used to combine the aesthetic characteristics of lithium disilicate and the strength characteristics of zirconia has shown promise. The aim of this thesis was to characterize the interface between lithium disilicate and zirconia produced in the “CAD-on” technique and establish the mode of failure. A better understanding of mode of failure may assist developers in strengthening future materials.

## **Preface**

With the exception of the control group, all components of this project, including research, test sample preparation, and dissertation writing, were completed without collaboration, apart from the help obtained from my supervisor, Dr. N. Dorin Ruse. He provided expertise and guidance with sample testing, biomaterial properties, and statistical analysis. Other committee members were Dr. Anthony McCullagh from the Faculty of Dentistry, and Dr. Tom Troczynski from the Department of Materials Engineering. This research project did not involve human or animal subjects and bio-hazardous materials and therefore did not require ethics board approval.

# Table of Contents

<b>Abstract</b> .....	<b>ii</b>
<b>Lay Summary</b> .....	<b>iv</b>
<b>Preface</b> .....	<b>v</b>
<b>List of Tables</b> .....	<b>vii</b>
<b>List of Figures</b> .....	<b>viii</b>
<b>List of Equations</b> .....	<b>x</b>
<b>List of Abbreviations</b> .....	<b>xi</b>
<b>Acknowledgements</b> .....	<b>xii</b>
<b>Dedication</b> .....	<b>xiii</b>
<b>Chapter 1: Introduction</b> .....	<b>1</b>
1.1. Ceramics and Glasses.....	3
1.2. Dental Ceramics .....	4
1.3. Computer Aided Design / Computer Aided Manufacturing .....	14
1.4. Testing Methods.....	23
<b>Chapter 2: Specific Aim</b> .....	<b>31</b>
2.1. Null Hypothesis.....	31
<b>Chapter 3: Materials</b> .....	<b>32</b>
3.1. IPS e.max CAD.....	32
3.2. IPS e.max ZirCAD .....	34
3.3. Crystal Connect™ .....	35
3.4. IPS e.max ZirPress .....	36
3.5. ZirLiner .....	38
<b>Chapter 4: Methods</b> .....	<b>39</b>
4.1. Sample Size Calculation .....	39
4.2. Experimental Design.....	40
4.3. Sample Preparation .....	41
4.4. Alignment and Glass Fusion (Test Groups).....	43
4.5. Control Sample Production .....	45
4.6. Interfacial $K_{IC}$ Determination .....	51
4.7. Light Microscopy Investigation .....	53
4.8. Scanning Electron Microscopy .....	54
4.9. Statistical Analysis .....	55
<b>Chapter 5: Results</b> .....	<b>56</b>
5.1. Interfacial $K_{IC}$ .....	56
5.2. Scanning Electron Microscopy .....	60
<b>Chapter 6: Discussion</b> .....	<b>66</b>
<b>Chapter 7: Conclusions</b> .....	<b>70</b>
<b>References</b> .....	<b>71</b>

## List of Tables

Table 1: Experimental materials .....	32
Table 2: Composition of IPS e.max CAD .....	33
Table 3: Composition of IPS e.max ZirCAD.....	35
Table 4: Composition of IPS e.max ZirPress and IPS e.amx ZirLiner.....	37
Table 5: Experimental design .....	40
Table 6: Press Parameters for IPS e.max ZirPress.....	50
Table 7: Test groups and mean $K_{IC}$ .....	56
Table 8: Weibull modulus and Weibull $K_{IC}$ .....	57
Table 9: Scheffe multiple comparison test.....	58

## List of Figures

Figure 1: Crystal phases and transition temperatures of zirconia .....	11
Figure 2: CAD/CAM workflow .....	15
Figure 3: Digital design of a “CAD-on” multi-unit restoration .....	18
Figure 4: Digital design of Y-TZP framework and overlying LS2 veneer.....	18
Figure 5: Framework components .....	19
Figure 6: Steps in production .....	20
Figure 7: Notchless Triangular Prism specimen $K_{IC}$ Test .....	29
Figure 8: IPS e.max CAD .....	32
Figure 9: IPS e.max partially and fully crystalized states.....	33
Figure 10: IPS e.max ZirCAD .....	34
Figure 11: Microstructure of (a) presintered and (b) sintered IPS e.max Zir CAD.....	35
Figure 12: IPS e.max ZirPress ingot .....	36
Figure 13: Variation of crystal size within IPS e.max ZirPress.....	37
Figure 14: Low speed Isomet saw .....	42
Figure 15: Cutting steps of IPS e.max CAD NTP half specimens .....	42
Figure 16: Grinding and section steps of the IPS e.max CAD half specimen .....	43
Figure 17: Alignment and luting of the NTP test half specimens.....	44
Figure 18: Glass fusion and crystallization of an LS2 – CC – LS2 NTP test specimens (A) Before crystallization (B) After crystallization .....	45
Figure 19: IPS e.max ZirLiner materials and application.....	46
Figure 20: IPS e.max ZirPress wax mould with ZirCAD half specimen and clear template disassembled mould. (D) Assembled wax mould.....	47
Figure 21: ZirPress sprueing guidelines .....	48
Figure 22: IPS e.max ZirPress sprueing and investment sequence .....	49
Figure 23: IPS e.max ZirPress firing and pressing sequence.....	49
Figure 24: IPS e.max divestment and finishing sequence .....	51
Figure 25: NTP test sample loading and defect creation .....	52
Figure 26: NTP holder/testing .....	53
Figure 27: Specimen holder and fractured samples .....	54

Figure 28: SEM and SEM samples .....	55
Figure 29: Graphical representation of Weibull analysis results .....	59
Figure 30: Box of the comparing interfacial $K_{IC}$ and test groups SEM analysis.....	59
Figure 31: IPS e.max ZirCAD NTP test half sample prior to glass fusion.....	60
Figure 32: IPS e.max CAD NTP test half sample prior to glass fusion.....	61
Figure 33: Two corresponding IPS e.max CAD NTP test half samples after fracture .....	62
Figure 34: Two corresponding IPS e.max ZirCAD NTP test half samples after fracture .....	63
Figure 35: ZirCAD e.max CAD (“CAD-on”) complex fracture sample .....	64
Figure 36: IPS e.max ZirCAD with ZirPress (control).....	65

## List of Equations

Equation 1: Irwin's (1957) fracture mechanics formula modification .....	25
Equation 2: Irwin's introduction of the stress intensity factor equation .....	26
Equation 3: Stress intensity factor formulas for three direct types (modes) of loading .....	26
Equation 4 A & B: $K_{IC}$ formulas with modulus of elasticity E and energy release rate for a plane stress and plane strain condition .....	27
Equation 5: $K_{IC}$ formula used by the CNSR and NTP fracture toughness tests.....	30
Equation 6: Lehr's basic Rule of Thumb equation .....	39
Equation 7: Fracture probability of a ceramic .....	39
Equation 8: Weibull formula producing graphic and Weibull modulus.....	55

## List of Abbreviations

CAD – Computer aided design

CAD-on – Term describing process of layering a zirconium substructure with a lithium disilicate veneer via glass fusion.

CAM – Computer aided manufacturing

CC – Connecting Glass

CEREC - Chairside economical restorations of esthetic ceramics

CNSR – Chevron notched short rod

CTE - coefficient of thermal expansion

FDP – Fixed Dental Prosthesis

$K_{IC}$  - Fracture toughness

LS2 – Lithium disilicate

MCC – Metal ceramic crown

NTP – Notchless triangular prism

SEM – Scanning electron microscope

Y-TZP – Yttrium oxide partially stabilized tetragonal zirconia polycrystal

SENB - Single edged notched beam test

FPB - Four point bend

## **Acknowledgements**

I would like to express my deepest thanks and gratitude to my supervisor Dr. N. Dorin Ruse for his continued support and guidance throughout this thesis project. His ability to reason through problems and focus my attention was instrumental in the completion of this work.

Also, I would like to thank my committee members Dr. Anthony McCullagh and Dr. Tom Troczynski for their interest, encouragement, and constructive feedback throughout the research process.

I also want to acknowledge the financial support I received from the Royal Canadian Dental Corps. I am honored to be a part of an organization with a long and proud tradition in dentistry and look forward to putting my training to use through future service.

## **Dedication**

This thesis is dedicated to my beautiful wife and editor Amber, who was beside me throughout every part of my journey through dental school and the Canadian Forces. Without her personal sacrifice, hard work, emotional support, and thoughtful insight, none of my success would have been possible.

## Chapter 1: Introduction

The metal ceramic crown (MCC) has been the gold standard for full coverage dental restorations in the aesthetic zone. Factors contributing to its 'success' include survival rates that approach 95% after 10 years, conservative tooth reduction requirements, predictable aesthetics, and excellent marginal adaptation.<sup>1,2</sup> Although MCC is still a frequently used restoration, persistent demands for restorations that are stronger, more natural looking, and more easily produced have pushed researchers/manufacturers to develop new materials/new techniques. Improvements in milling and scanning capabilities, dentinal bonding, and the integration of digital design have helped dentists, laboratory technicians, and manufactures explore different restorative materials that meet these changing requirements.

e.max CAD (Ivolar Vivadent, Schaan, Lichtenstein), a lithium disilicate glass-ceramic (LS2), and e.max ZirCAD (Ivolar Vivadent, Schaan, Lichtenstein), composed of yttria tetragonal zirconia polycrystal (Y-TZP), are two examples of newer millable dental materials. Both zirconia and lithium disilicate are strong, aesthetic, and relatively well suited for various roles in CAD/CAM dentistry. As a material, LS2 has been advocated for use in inlays, onlays, anterior single crowns, anterior multi-unit FDPs, posterior crowns, and implant supported crowns.<sup>3</sup> e.max CAD single crowns have been reported to perform similarly to conventional metal-based restorations in anterior regions, and have earned a reputation as being reliable and esthetic.<sup>4,5</sup> Translucency, biocompatibility, and ease of production through digital design are additional favourable properties exhibited by LS2.<sup>6,7</sup> Nevertheless, restorative failures, such as chipping and framework fractures, continue to limit its use in posterior regions of the mouth.<sup>8,9</sup> Efforts to reduce failures

through improved firing protocols,<sup>10</sup> coping and framework modifications,<sup>11</sup> and altered processing techniques have yielded mixed results.<sup>12</sup>

Zirconia restorations, such as e.max ZirCAD, have also garnered positive attention for their restorative characteristics and milling capability.<sup>13</sup> A flexural strength exceeding all other dental restorative ceramics, a white colouration, and the capacity to resist crack propagation make it a strong candidate as a restorative material for multi-unit restorative frameworks and implant supported restorations.<sup>14-16</sup> Many practitioners have begun to adopt Y-TZP as a choice for multi-unit and posterior restorations.<sup>17</sup> Unfortunately, an opaque finish, and a lack of translucency have meant that Y-TZP often requires veneering with a second ceramic to achieve acceptable esthetic results.<sup>18</sup> Poor veneer adhesion to Y-TZP, resulting in restoration failures in the form of veneer chipping or complete veneer fracture, has been the principal cause of clinical failures in Y-TZP based restorations.<sup>18-21</sup> Ideally, the development of a restorative material that could combine the aesthetic characteristics of LS2 and the strength characteristics of zirconia would produce a restoration that could satisfy the aesthetic requirements while maintaining the ability to survive in all areas of the oral cavity.<sup>22</sup>

In an effort to improve upon the translucency, aesthetics, and durability of zirconia-based restorations, Ivoclar Vivadent has developed a method of layering ceramic frameworks, called “CAD-on”.<sup>22</sup> Restorations produced through this technique consist of a bi-layered structure composed of a CAD/CAM processed IPS e.max CAD LS2 veneer that is glass-fused to a CAD/CAM processed IPS e.max ZirCAD Y-TZP framework. The “CAD-on” technique was developed on the premise that the commercially produced ceramic used in the veneer would

possess fewer flaws, be more resistant to fracture, and be easily manufactured in comparison to hand or pressed veneers<sup>23,24</sup>. It was hypothesized that the combination of the LS2 veneer and a Y-TZP framework would (1) reinforce the veneer, resulting in a restoration more resistant to failure than those created using current zirconia veneering techniques, and (2) provide more translucency than conventional metal ceramic restorations. Research in the area of CAD/CAM manufactured veneers, or “CAD-on technique” for fixed dental prostheses is limited but the principle ideas appear to hold promise. Exploring and characterizing the glass fusion layer as it applies to fixed dental prosthesis (FDP) would aid in the evaluation of the “CAD-on” technique and better enable clinicians to make an evidence based decision regarding material and restoration selection.

### **1.1. Ceramics and Glasses**

According to Smith<sup>25</sup>, the term ceramic refers to “crystalline, inorganic, non-metallic materials which consist of metallic and non-metallic elements bonded together primarily by ionic and covalent bonds”. Philips<sup>26</sup> refers to a dental ceramic as a group of materials “consisting of silicate glasses, porcelains, glass ceramics, or highly crystalline solids.” Different from a ceramics, glasses do not form crystalline solids upon cooling, are amorphous, and resemble frozen solutions.<sup>27</sup> Powers et al.<sup>28</sup> define a glass as “a non-metallic, inorganic solid in which elements are heated to fusion then cooled to a rigid solid without crystallization.”

Ceramics have played important roles in human history, culture, and technology, are among the most important artefacts found at archaeological sites.<sup>29</sup> The first use of ceramics, when humans discovered that clay could be formed into objects, dates back to the late Palaeolithic period in central and western Europe, where fired and unfired clay figurines were created as a form of artistic expression.<sup>30</sup> The basic materials of these early ceramics are readily found in the natural

environment and consist of silica, clay, and feldspar. Silica is the basic component of traditional ceramics and glasses and is formed when all four oxygen atoms are shared between adjacent silicate tetrahedra to form a three dimensional crystalline network.<sup>26</sup>

Kaolinite (pure clay), classified as a phyllosilicate or sheet silicate, consists of a negatively charged sheet of silica ( $\text{Si}_2\text{O}_5$ )<sup>2-</sup> and a positively charged sheet of aluminum hydroxide [ $\text{Al}_2(\text{OH})_4$ ]<sup>2+</sup>.<sup>26</sup> When exposed to water, the alternating layers of silica and aluminum hydroxide become loosely bound and are able to slide past one another. This sliding of sheets is the characteristic which allows potters to mold clay into objects.<sup>27</sup> The elimination of water during firing forms a glassy matrix, turning the clay into objects such as tools, ornaments and porcelain dinnerware.<sup>27</sup> The term “porcelain” is generally used for ceramics produced with a significant amount of kaolinite.<sup>26, 28</sup> Although “porcelain” is often used to describe dental ceramics, they no longer contain clay.<sup>31</sup>

In feldspars,  $\text{Al}^{(+3)}$  replaces  $\text{Si}^{(+4)}$  within the silica network, leading to a negatively charged structure. To balance the charges, cationic species, such as  $\text{Na}^+$ ,  $\text{K}^+$ ,  $\text{Ca}^{2+}$ , need to be incorporated into the network. Feldspars could be either amorphous or crystalline and have variable melting temperatures. In ceramics, feldspars are responsible for forming the glassy matrix into which silica acts as a refractory filler. Changing the feldspar/silica ratio can be used to control the properties of ceramics, such as coefficient of thermal expansion (CTE), melting, and transition temperatures.<sup>32</sup>

## 1.2. Dental Ceramics

Dental ceramics are important as restorative materials because of their biocompatibility, colour stability, durability, and wear characteristics.<sup>26</sup> The use of traditional feldspathic ceramics in

dentistry can be traced back to the mid eighteenth century with the advent of the porcelain jacket crown.<sup>15</sup> Utilizing a burnished platinum foil substructure, Charles Land was able to produce the first fused feldspathic all ceramic restoration in 1885.<sup>15</sup> These “porcelain jacket” restorations had compositions similar to clay pottery ceramics, lacked strength, were prone to fracture, and were limited to the esthetic areas.<sup>33,34</sup>

Arguably, one of the most significant advancements in dental ceramics was the advent and enhancement of the modern MCC.<sup>26</sup> Although initial attempts to chemically bond feldspathic porcelains to metallic copings were unpredictable, several prominent developments had important implications on ceramic restorations and allowed MCC to become “the gold standard” in esthetic dentistry.<sup>26 34</sup> The most significant development was increasing the CTE of feldspathic ceramics by the incorporation of leucite.<sup>34</sup> Leucite ( $K_2O \cdot Al_2O_3 \cdot 4SiO_2$ ) has a relatively high CTE, between (20 – 25) ppm/K.<sup>35</sup> When added to feldspathic ceramic, leucite crystallizes and raises the overall CTE of the feldspathic ceramic. The CTE of the alloys used in dentistry typically range from 13.8 – 15.0 ppm/K.<sup>26</sup> By adjusting the concentrations of soda, potash, and leucite, manufacturers were able to adjust CTE of the feldspathic ceramics to just under the CTE of the intended metal coping.<sup>26</sup> This slight difference between CTE places the ceramic in compression, which improves resistance to fracture.<sup>36</sup> The second development was the production of alloys thermally compatible with the newly developed feldspathic ceramics.<sup>34 26</sup>

Despite the prolonged success of MCC, complications such as ceramic fracture, lack of translucency, margin discolouration, and metal allergies, have continued to drive the development of new materials.<sup>12, 19, 23, 37</sup> There has been a significant shift toward all ceramic restorations as their

popularity continues to increase.<sup>7,19,38,39</sup> Early all ceramic restorations lacked the strength required to withstand the higher posterior masticatory forces and were used primarily for esthetic restorations in the anterior region.<sup>26,34</sup> Newer all-ceramic crowns, however, are being used in the posterior dentition as well. Some authors have even suggested that posterior all-ceramic restorations are as reliable as MCCs.<sup>40</sup>

### **1.2.1. Glass Ceramics**

Many of the all-ceramic restorative systems, especially those produced for anterior esthetic regions, are made from feldspathic glass ceramics. They are classified as glass-ceramics and differ from early conventional dental porcelains in their production through controlled crystallization and lack of clay.<sup>31,41</sup> The controlled crystallization of the glass, which results from the thermo-regulated nucleation and growth of internal crystals, results in crystals that are evenly distributed throughout the glass matrix.<sup>32</sup> This creates a glass-ceramic that contains an amorphous feldspathic glass matrix reinforced with silica and crystallized fillers.<sup>42</sup> The number of crystals, their growth rate and thus their size are regulated by the time and temperature of the heat treatment.<sup>32</sup> By modifying the glass matrix and filler compositions, developers have been able to create dental glass-ceramics with improved mechanical properties for both metal ceramic and all-ceramic restorations.<sup>26</sup> An important example of this was the addition of leucite into feldspathic ceramic. Upon cooling, the discrepancy in thermal contraction between leucite crystals (20 to 25 ppm/K) and the glassy matrix (8 ppm/K) leads to peripheral compressive forces in the glass surrounding the leucite crystals and helps to impede crack propagation.<sup>31</sup> Other examples of fillers that have been precipitated to improve the mechanical properties include mica, found in Dicor, (Dentsply) fluorapatite, found in Vita Mark series (Vita ZahnFabrik), leucite, found in IPS Empress and IPS ProCad (Ivoclar Vivadent), and LS2 in the IPS e.max (Ivoclar Vivadent) series<sup>26,31,43</sup>,

a newer restorative glass-ceramic that has become increasingly popular since its introduction.<sup>9</sup>

#### **1.2.1.1. Lithium Disilicate**

Developed by Ivoclar Vivadent in 1998, LS2 was first marketed as Empress 2. Empress 2 was replaced and rebranded in 2001 as IPS e.max Press.<sup>26</sup> IPS e.max CAD, a millable form of LS2 glass-ceramic was released in 2005.<sup>43</sup> e.max CAD has a smaller and more densely packed crystalline structure than its Empress 2 predecessor. Restorations made from both versions of e.max contain approximately 65-70% by volume  $LS_2$  crystals.<sup>26,43</sup> The size of the crystals in both e.max ceramics can range in size from  $0.5 \mu\text{m}$  to  $4.0 \mu\text{m}$  and are dispersed in a feldspathic glassy matrix.<sup>43,44</sup> The crystals, which affect the translucency and strength of the restorations, can be controlled by the constituents of the glassy matrix and the temperature during heat treatment.<sup>45</sup> Empress 2, e.max Press, and e.max CAD have reported flexural strengths ranging from (260 – 400) MPa.<sup>26,31,43</sup> Several investigations of LS2 have reported K<sub>IC</sub> values ranging between (1.8 – 3.0) MPa·m<sup>1/2</sup>.<sup>7,46,45,47</sup> Since its development, LS2 has been routinely used to produce both single crowns and multi-unit FDPs. According to the manufacturer, this material is indicated for anterior laminate veneers, single crowns, and three unit FDPs to the second premolar.<sup>43</sup>

e.max Press and e.max CAD ceramics have two distinct processing pathways. e.max Press is supplied as ingots of  $LS_2$  glass ceramic and is processed by utilizing the lost wax technique, i.e. restorations are waxed to the desired contours, sprued, and invested. After investing, the molten ceramic (e.max Press) is forced into the mold in a specially designed furnace.<sup>48</sup> e.max CAD is processed by CAD/CAM methodology. Initially, the material is cast in a one-piece transparent glass ingot.<sup>43</sup> The ingots are then partially crystallized to form lithium metasilicate crystals within the glassy matrix. The metasilicate crystals range in size from  $0.2 \mu\text{m}$  to  $1.0 \mu\text{m}$ .<sup>22</sup> The partially

crystallized blocks do not possess the same degree of strength and hardness as the fully crystallized blocks, making them more suitable for milling. Upon completion of milling, the contour and anatomy of the restoration is verified and adjusted intraorally. A specific firing protocol is then used to fully crystallize the restoration. In the final crystallization process, the lithium metasilicate crystals are converted into LS2 crystals.<sup>43</sup>

There have been few controlled clinical trials involving LS<sub>2</sub> restorations. Most of existing investigations have been over relatively short periods of time, ranging between 3 to 6 years. Nevertheless, several patterns appear to emerge from the literature. Anterior and monolithic single unit crowns have short-term success and survival rates similar to those of MCCs, ranging between 95% – 100%.<sup>49,50</sup> Short term cumulative failure rates for anterior and posterior layered single unit crowns, which range between 0% - 4.1%, appear to meet or exceed the results seen in single unit MCCs.<sup>51,52</sup> LS2 multi-unit FDPs do not appear to possess the same degree of reliability as single unit LS2 restorations or MCC FDPs. Despite strong relative flexural strength, LS2 framework fracture and veneer chipping have been associated with multi-unit restorations in posterior regions.<sup>53-55</sup> After 10 years of function, investigations reported complication rates in posterior FDPs to be as high as 33%.<sup>53, 56</sup> Efforts to produce larger restorations with reduced chipping and improved firing protocols<sup>10</sup> and framework modifications<sup>11</sup> have had mixed results. Experimentation with veneering techniques involving pressed and CAD protocols have also yielded mediocre results.<sup>12</sup>

### **1.2.2. Industrial Ceramics**

Posterior all-ceramic restorations face greater occlusal stresses and have been found to have higher failure rates.<sup>4,57</sup> Some authors have suggested that feldspathic and glass ceramics should be limited

to single crowns, anterior FDPs, or veneering in posterior regions.<sup>38, 40, 58</sup> Limiting the role of feldspathic ceramics to lower force areas, or as veneering ceramics, restricts the all-ceramic restorative options for the posterior dentition. Stronger, less esthetic industrial ceramics have been used as posterior restorative materials.<sup>26, 31</sup> Some of these stronger ceramics include glass-infiltrated ceramics, such as In-Ceram Spinell, In-Ceram Alumina, and In-Ceram Zirconia (VITA Zahnfabrik, Bad Sackingen, Germany).<sup>40</sup> Other strong ceramics restoration include the industrial pure monophase ceramics of alumina and zirconia.<sup>41, 59</sup>

The In-Ceram series (VITA Zahnfabrik, Bad Sackingen, Germany) are glass-infiltrated high strength ceramic core systems.<sup>26, 41</sup> These infiltrated ceramic systems are made through a process called slip-casting where an aqueous ceramic slurry is formed into a porous core on an oversized refractory die<sup>26, 60</sup> After sintering, the cores are infiltrated with lanthanum glass via capillary action to improve translucency and produce a strong dense ceramic coping or framework.<sup>40</sup> The glass-infiltrated cores are then veneered with an esthetic feldspathic ceramic to obtain the final shade and desired anatomy.<sup>41, 60</sup> In-Ceram Alumina, the oldest of the three infiltrated systems, is composed of aluminum oxide (~60% vol) framework and lanthanum glass.<sup>26, 41</sup> In-Ceram Alumina is reported to have a flexural strength of  $(590 \pm 52)$  MPa and a  $K_{IC}$  of  $3.9 \text{ MPa}\cdot\text{m}^{1/2}$ .<sup>26, 61</sup> In-Ceram Spinell, which was developed to overcome the low degree of translucency of In Ceram Alumina, has a crystalline core ceramic combination composed of magnesia and alumina (roughly 70% vol). In-Ceram Spinell has a lower flexural strength than In Ceram alumina (350 MPa), limiting its use to single crowns and anterior multi-unit FDPs.<sup>62</sup> In Ceram Zirconia, the newest of the glass infiltrated ceramics, is composed of 62% alumina, 20% zirconia, and 18% infiltrated glass.<sup>60</sup> This restorative material was developed for posterior frameworks and has flexural strength of  $630 \pm 58$

MPa.<sup>63</sup> Although In-Ceram Zirconia restorations have had favourable results in the posterior region, investigations have revealed significant amounts of veneer chipping and lower flexural strengths than monophase zirconia.<sup>5, 26, 64</sup>

Industrial pure monophase ceramics, such as alumina and zirconia, consist of dense polycrystalline structures, which lack a glass matrix.<sup>41, 59</sup> Alumina and zirconia ceramics are two of the strongest ceramics used in dentistry.<sup>26</sup> Because of their density and lack of glass component, these materials are particularly opaque and are ordinarily veneered with an esthetic ceramic. Procera (Nobel Biocare AB, Goteborg, Sweden), the first and most prominent of the alumina based restorations, was developed in 1993 and consists of 99.9% high purity aluminum oxide.<sup>60</sup> Procera restorations possess flexural strengths of 620 MPa to 700 MPa and  $K_{IC}$  values of  $\sim 4.8 \text{ MPa}\cdot\text{m}^{1/2}$ , exceeded only by zirconia based restorations.

Zirconia, which has been advocated for single unit crowns, multi-unit FDPs, and complete mouth rehabilitation, has seen unprecedented popularity among dental restorative materials.<sup>65, 66, 71</sup> This popularity is due in part to the success zirconia based restorations have had in posterior regions of the mouth. The popularity has also been bolstered by advances in CAD/CAM technologies and zirconia's ability to be paired with an aesthetic veneer, or left in a monolithic form where veneer chipping is a concern. Compared with alumina, zirconia has higher  $K_{IC}$  and flexural strength and lower modulus of elasticity and hardness.<sup>26, 67</sup>

#### **1.2.2.1. Zirconia**

Zirconia is a polymorphic material that is capable of existing in cubic, tetragonal, or monoclinic phases, depending on temperature.<sup>26</sup> Its high strength, light color, biocompatibility, and ease of

production through milling have made Y-TZP desirable for use in posterior restorations. Above 2367°C and below its melting point of 2680 °C, zirconia exists as a cubic structure. Between 2367°C and 1170°C zirconia exists in tetragonal form, and below 1170°C zirconia exists in monoclinic form (Figure 1).

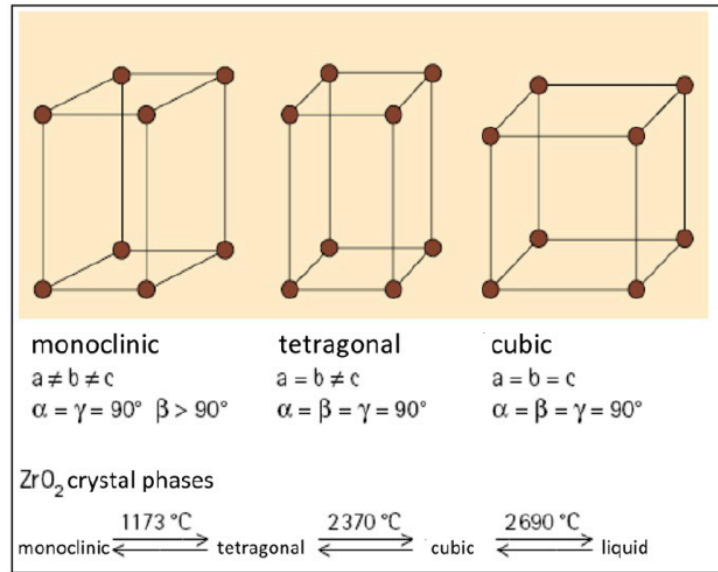


**Figure 1: Crystal phases and transition temperatures of zirconia<sup>22</sup>**

During the tetragonal to monoclinic phase change at 1170°C, there is a 3 – 5% increase in volume of the zirconia crystals. To prevent the zirconia crystals from transforming from tetragonal into monoclinic phase below 1170 °C, oxides of yttrium, magnesium, calcium, and cerium can be added.<sup>38, 68</sup> At room temperature, yttria stabilized tetragonal zirconia polycrystal (Y-TZP) possesses a dense tetragonal microcrystalline structure. This difference in crystalline structure between the tetragonal and monoclinic forms is thought to provide Y-TZP with the advantageous effect of tension induced transformation strengthening, where a phase change from (t → m) at the crack tip leads to an increase in volume. Phase transformation reduces the energy at the tip of the crack while simultaneously compressing the flanks of the crack, acting to prevent further crack

growth and giving the material exceptional  $K_{IC}$  and flexural strength.<sup>69</sup> Although other stabilizers have been used to stabilize zirconia, Y-TZP, has been the most commonly used form of zirconia for dental restorations. Y-TZP restorations have been reported to have flexural strengths ranging between (800 – 1300) MPa<sup>28</sup> and  $K_{IC}$  ranging between (5 - 10.3) MPa·m<sup>1/2</sup>.<sup>70, 71</sup> When compared with the alumina and glass infiltrated moduli of elasticity between 250 GPa and 310 GPa, Zirconia's modulus (200 GPa to 210 GPa) is closer to that of enamel (84 GPa), making it more suited to reinforce tooth structure.<sup>67, 72</sup> Y-TZP can be milled in its unsintered, partially sintered, or fully sintered forms. Most restorations are milled prior to sintering in order to reduce milling time and instrument wear. E.max ZirCAD, a material used in this thesis, was introduced in 2006 as a pre-sintered Y-TZP ingot designed for use in both laboratory and chairside milling devices.

#### **1.2.2.2. Zirconia Veneering**

To overcome the high degree of opacity, zirconia restorations are veneered with feldspathic ceramics. The desired effect of combining an esthetic translucent ceramic veneer over the zirconia framework is to produce a restoration with the strength and toughness of zirconia and the esthetics of the veneering porcelain. Two conventional methods have been established for veneering zirconia FDP frameworks. These methods are the layering technique and the heat pressing technique.<sup>5, 73</sup> The layering technique involves the gradual build-up of the veneer ceramic via the application of ceramic powder to the zirconia framework. Ceramic powder is mixed with a wetting agent and applied via a fine brush.<sup>26</sup> The veneer is built up through small increments and multiple sintering steps.<sup>26</sup> The heat pressing technique involves the investment of the desired veneer pattern on the zirconia framework. The invested pattern is preheated, burned out, and transferred to a furnace where an ingot of veneering ceramic is pneumatically pressed into the investment.<sup>48, 74</sup> The exact bond mechanism between the zirconia and the glass ceramic remains unproven.<sup>13</sup> Several

authors have suggested a mechanical engagement exists due to the formation of compressive stresses resulting from thermal contraction during cooling after sintering.<sup>13,75</sup>

Both veneering methods have weaknesses. The layering method has been reported to be more prone to errors, specifically due to the incorporation of air or defects between layers during mixing, or thermal induced stress due to multiple firings.<sup>26,76</sup> Shear bond strengths approaching 8.0 MPa have been reported for the layered method while shear bond strengths in the range of 13.0 MPa have been reported for the pressed method.<sup>73</sup> The pressed method is reported to be technique sensitive, with the potential for voids being produced at the framework interface.<sup>73</sup> Several studies have made comparisons between the physical and clinical performances of the pressed and layered veneering systems. Some recent investigation include those by Lopez-Molla et al.<sup>76</sup>, Lopez-Molla et al.<sup>77</sup>, Subash et al.<sup>73</sup>, and Stawarczyk et al.<sup>78</sup> The degree to which one method is superior to another is questionable.<sup>79</sup> Differences in ceramics, firing and cooling rates, veneer thickness, framework designs, and veneering techniques make comparisons difficult. However, the heat pressed veneering techniques have demonstrated higher values in the areas of shear bond strength, consistency, load-bearing capacity, flexural strength, and core adaptation.<sup>73,</sup>

<sup>76,78</sup>

The feldspathic veneering, with flexural strength ranging between 90 MPa to 125 MPa, are significantly weaker than the underlying framework. Veneer chipping and fracture has been cited as a principle cause of failure for zirconia based restorations.<sup>37, 39, 67, 80</sup> Differences in the failure mechanism have been reported. Cracking has been reported to originate within the veneering layer, and has been described as propagating along the zirconia coping interface.<sup>39, 61</sup> Others have

reported clinical failures that originate in the veneering ceramic with the crack propagating throughout the ceramic restoration.<sup>39</sup> Veneer fracture rates have been reported as high as 9% for single crowns after 6 months and as high as 20 - 30% over 5 – 10 years.<sup>17, 81, 82</sup> Two prominent modes of veneer failure have been reported within the literature. These include cohesive failure within the veneering ceramic and adhesive failure at the veneer and framework interface.<sup>17, 19, 83, 74</sup> Factors affecting veneer strength include the production method, framework wettability, the veneer ceramic, and residual stresses at the interface.<sup>84, 85</sup> Other factors include firing and cooling cycles, cooling rates, thermal expansion coefficients, and framework design.<sup>84, 85</sup>

### **1.3. Computer Aided Design / Computer Aided Manufacturing**

Computer aided design and computer aided manufacturing (CAD/CAM) in dentistry has evolved significantly since its introduction almost four decades ago.<sup>86</sup> Accepted by most clinicians as a suitable treatment option for numerous restorative scenarios, CAD/CAM technology can convert ceramic or composite blocks into dental restorations. Arguably, this digital methodology significantly reduces treatment time and laboratory costs.<sup>87</sup> Depending on workflow (Figure 2), an optical impression is created from an intra oral camera or a cast scanner.

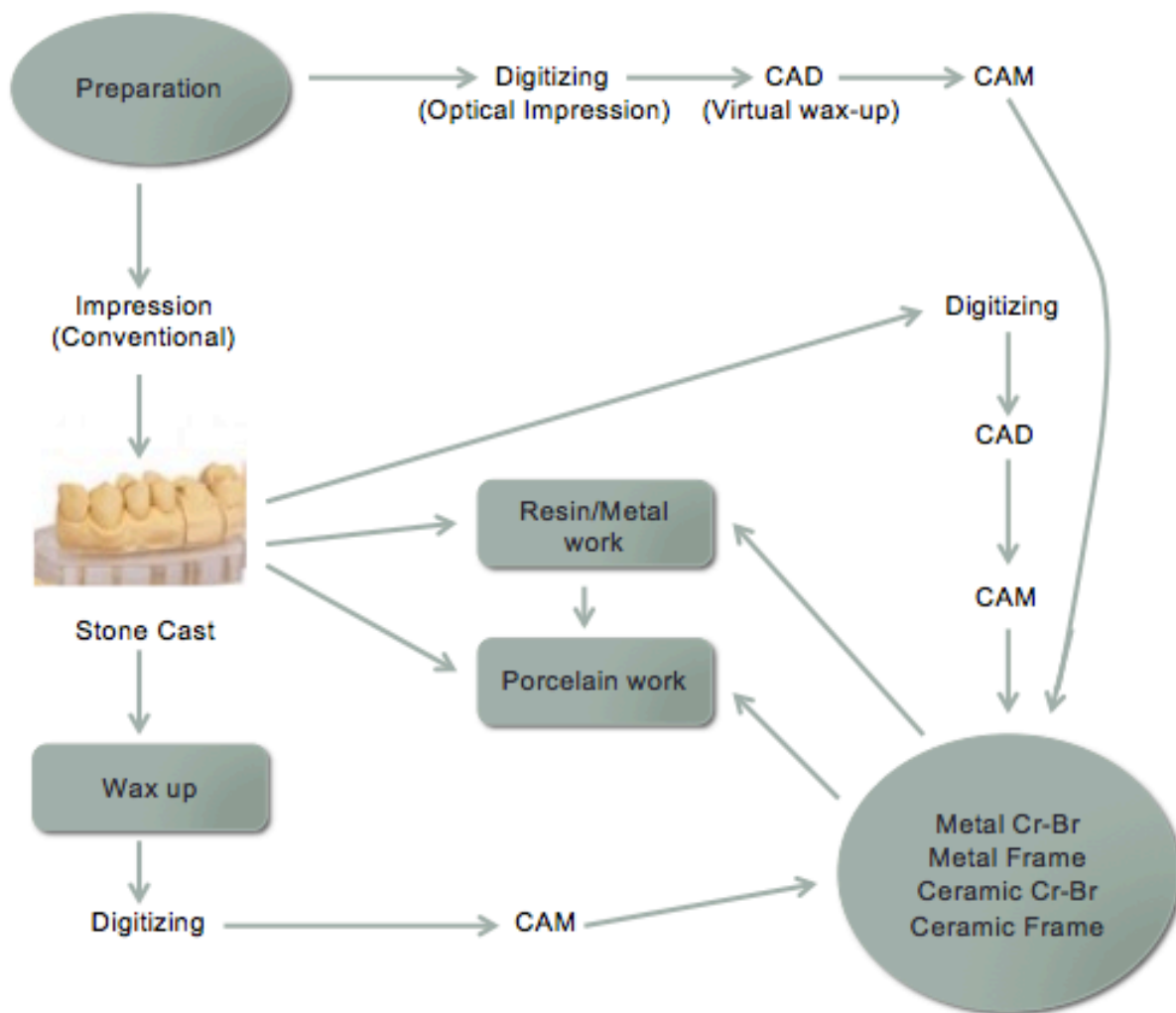


**Figure 2: CAD/CAM workflow**<sup>88</sup>

The analyzed image is processed through design software to create a 3-dimensional (3D) model of the prepared tooth or implant abutment. The model is then used to digitally design the restoration from a massive anatomical catalogue, which is then refined by the practitioner or technician. To accurately design the definitive restoration, the morphology of adjacent teeth, abutment, preparation margins, and opposing teeth must be accurately incorporated into the digital model.<sup>89</sup> After the restoration model is refined, the design contains the necessary data to create the

restoration. The data is transferred to a milling machine which mills the designed restoration from a block made from the desired restorative material. Depending on the milling system and the size of the restoration, milling can take anywhere from 10 to 30 minutes to complete. Generally conducted under irrigation, two or more burs reduce the block of material by removing the excess until only the restoration remains.<sup>89</sup>

### **1.3.1. “CAD-on”**

“CAD-on” was developed by Ivoclar Vivadent as a method of sintering together a milled ceramic veneer with a milled ceramic framework. The aim of this new technique was to reduce the problems encountered with the layering and pressed approaches. The “CAD-on” production method is similar to the workflow involved with conventional milled all-ceramic restorations. The manufacturer claims that “CAD-on” restorations are capable of withstanding high occlusal loads without sacrificing translucency or aesthetics, which are often lost in monolithic zirconia restorations.<sup>22</sup> The IPS e.max “CAD-on” technique combines two CAD/CAM materials, IPS e.max ZirCAD and IPS e.max CAD, with a glass fusing ceramic, called “crystal connect”. In this process, IPS e.max ZirCAD acts as framework, and IPS e.max CAD (LS2) is used as the veneering structure. Traditionally, ZirCAD has been veneered, via a layering process, with IPS e.max Ceram or with IPS e.max ZirPress ceramic, using a lost wax press-on technique. “CAD-on” utilizes splint file milling to combine a LS2 veneer with a Y-TZP framework. According to the manufacturer, CC creates a homogenous bond between the surface of the framework and the surface of the veneer in a process Ivoclar Vivadent has called glass fusion.<sup>22</sup>

### **1.3.2. “CAD-on” Rationale**

The objective of “CAD-on” technology is to produce a restoration that is stronger and more translucent by successfully combining the aesthetic properties of LS2 veneer with the mechanical strength characteristics of Y-TZP framework. Unlike alloy-based restorations, “CAD-on” prostheses will not reveal a metal substructure if cracked or chipped, making “CAD-on” restorations more easily camouflaged and less apt to require replacement. Additionally, the production of any conventional FPD is usually done in part via casting, slip casting, or pressing. The ability to produce an FPD entirely from milling may reduce the amount of time and material required to produce the framework. In the case of “CAD-on”, the veneer and framework can be produced concurrently speeding up the process of the prosthesis.<sup>22</sup> In contrast, producing a conventionally pressed restoration involves wax-up, spruing, investing, burnout, and pressing. Each of these steps involves considerable time and work on the part of a technician. Wax-up and spruing a restoration contains an artistic component that is learned over several years and takes time to master. Replacing the diagnostic wax-up with digital rendering eliminates the investment medium, conserves laboratory time, and decreases the skill requirements of the technician. The preheating step involved in most pressing methodologies is also eliminated. Ivoclar Vivadent suggests that the “CAD-on” technique promotes efficiency by reducing the production time by a reported 40% over conventional pressed methods.<sup>22</sup> Finally, “CAD-on” FDPs utilize commercially produced ceramics, which have been reported to have fewer flaws or inclusions and are better able to resist fracture.<sup>23,24</sup>

### **1.3.3. “CAD-on” Fabrication**

To fabricate a “CAD-on” restoration, a scan of the tooth preparation or implant abutment is acquired, either through an intraoral scanner, or a scan of the poured casts. The restorations are

then designed digitally to full contour with complete anatomy, including occlusal and interproximal contacts (Figure 3).<sup>90</sup>

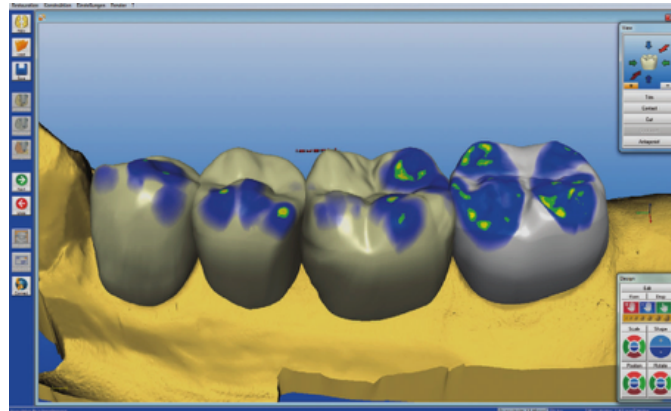


Figure 3: Digital design of a “CAD-on” multi-unit restoration<sup>22</sup>

After the completion of design, the data is split into different milling data sets, one file for the LS<sub>2</sub> veneer and a separate milling file for the Y-TZP framework (Figure 4).

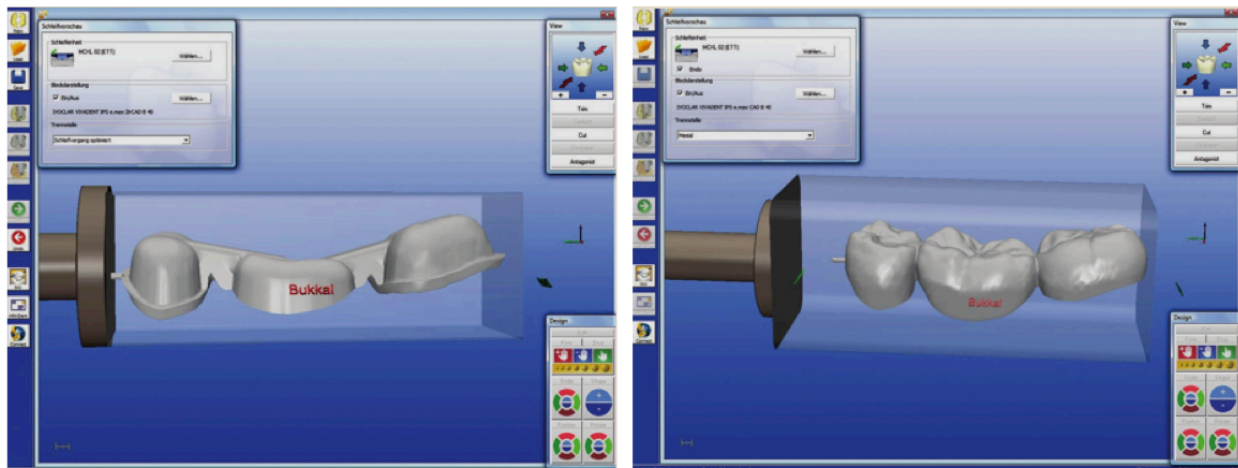
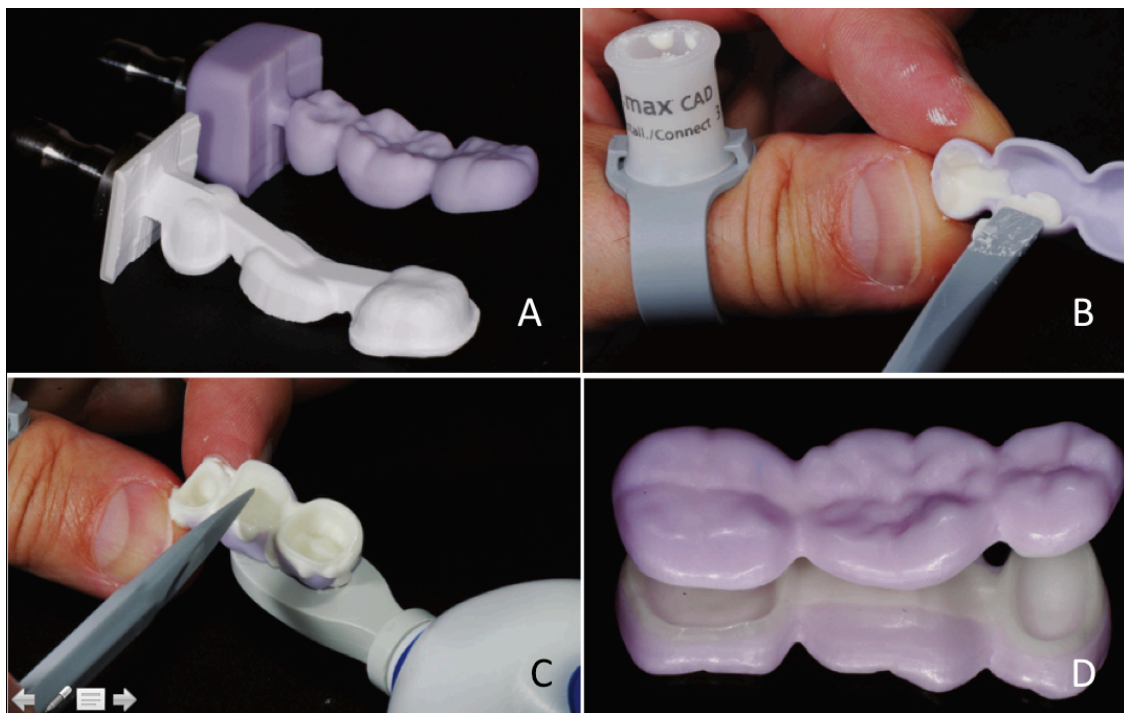


Figure 4: Digital design of Y-TZP framework and overlying LS<sub>2</sub> veneer<sup>90</sup>

Milling is then carried out separately, to produce the two components (Figure 5A). After cleaning and drying, the Y-TZP framework is fully sintered. Following Y-TZP sintering, the framework

and pre-crystallized LS2 veneer are checked to insure proper interdigitation between framework and veneer. If required, adjustments are made to the LS2 veneer. Following correct approximation of the two pieces, the occlusal and interproximal contacts of the restoration are verified and adjusted, either intraorally or with the use of an articulator. After final adjustments, the two pieces are joined together under vibration with the thixotropic glass intermediate (Figure 5 B). The CC substrate presents in the form of a pre-mixed moist paste. The intermediate is applied to the occlusal aspect of the framework and the underside of the veneer. Under vibration, the thixotropic glass slurry liquefies and allows the framework to settle into the veneer aided by finger pressure. During settling, excess crystal-connect material is expelled at the margin (Figure 5 C-D).<sup>22,90</sup>



**Figure 5: Framework components<sup>22</sup>**

- A) Milled Y-TZP framework and LS2 veneer
- B) Application of fusion intermediate
- C) Vibration coupling of the veneer and framework
- D) Layered restoration prior to LS2 crystallization

Fusion of the IPS e.max CAD veneering structure to the IPS e.max ZirCAD framework and the crystallisation of the IPS e.max CAD veneering structure occur simultaneously. According to Ivoclar Vivadent's literature<sup>91</sup>, the veneer and the fusing glass undergo crystallization and sintering simultaneously at approximately 840 °C (Figure 6A). After cooling, the restoration can be finished with a glaze or polished for aesthetics (Figure 6B).

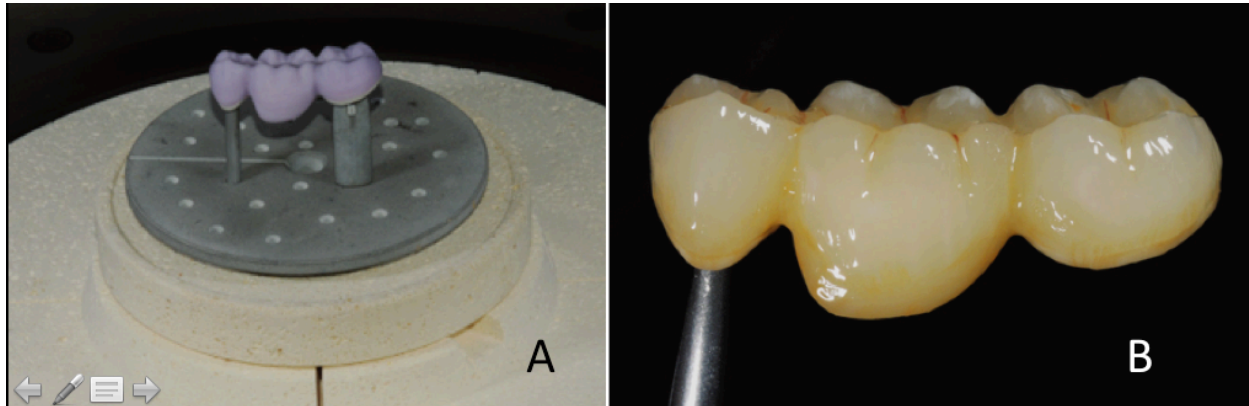


**Figure 6: Steps in production<sup>90</sup>**

- A) Concurrent glass fusion and crystallization of veneer
- B) Stained and glazed restoration

#### **1.3.4. “CAD-on” Literature**

Research in the “CAD-on” technique for fixed dental prostheses is limited. To date, investigations include analysis of cyclic stress profiles, flexural strengths, microtensile bond strengths, and fracture loads. Research conducted by Beuer et al.<sup>92</sup> in 2009 was the first independent trial to examine CAD/CAM-fabricated layered restorations. This study compared fracture loads of CAD produced veneers on Y-TZP copings and conventionally layered zirconia restorations. Prior to this investigation, the “CAD-on” protocol had not been released by Ivoclar Vivadent. In 2009, little standardized terminology, protocol, or software existed to allow for the use of “CAD-on” manufactured restoration. Therefore, the study by Beuer used adapted scanning technology

instead of the file splitting software used for present “CAD-on” restorations. The investigation also did not account for glass fusing ceramics or CC in their methodology, instead citing an experimental low fusing ceramic connecting material whose characteristics were not described. Beuer et al.<sup>92</sup> concluded that the CAD/CAM-fabricated layered restorations displayed significantly higher loads to fracture than the conventional techniques of layering and pressing. This research group also speculated that “CAD-on” veneering would offer the ability to produce cost-effective crowns and fixed partial dentures with a reduced risk of chipping.

A 2011 study by Schmitter et al.<sup>93</sup> was the first to conduct an independent investigation of the “CAD-on” technique in its present form. This investigation was also the first to describe the connecting ceramic as a glass fusion substrate. Schmitter et al.<sup>93</sup> utilized thermocycling and finite element modelling/finite element analysis (FEM/FEA) to compare manually layered zirconia restorations with CAD/CAM manufactured veneers. Similar to Beuer et al.<sup>92</sup>, results from this study suggested that “CAD-on” FPDs would be significantly more resistant to veneer fracture than conventionally veneered zirconia restorations. Like Beuer et al.<sup>92</sup>, this study also suggested that “CAD-on” veneered Y-TZP based restorations could be an efficient method of producing all ceramic restorations with fewer veneer failures.

In 2015, Basso et al.<sup>94</sup> attempted to examine the flexural strength,  $K_{Ic}$ , and failure behaviour of layered samples produced via “CAD-on” technique using a three-point bend test. The characteristic strength and  $K_{Ic}$  were statistically similar between monolithic and layered samples. The  $K_{Ic}$  values were significantly greater for the “CAD-on” group compared to the monolithic zirconia group. Following this study, in 2016, Basso et al.<sup>95</sup> examined the reliability and failure

behaviour of “CAD-on” layered specimens under fast fracture load and cyclic load. Under cyclic stress profiles, framework failure was the primary mode of failure. Under fast fracture stress profiles, veneer failure appeared more likely. After statistical analysis, the authors concluded that “the test method significantly influenced the reliability and fracture mechanism of FPDs fabricated using the “CAD-on” technique.

Nossair et al. (2015)<sup>96</sup> was the first to use fractographic analysis to examine the difference between “CAD-on” groups, glass fused groups, and a hand sintered control group. Each test group was exposed to axial forces. The “CAD-on” samples demonstrated significantly higher forces to failure over both the glass fused samples and the conventionally layered samples. Cemented “CAD-on” veneers appeared to fail due to cracking within the veneer and resin interfaces while the glass fused “CAD-on” LS2 underwent cohesive failure, usually initiating at the bulkiest portion of the glass interface. Nossair et al. (2015)<sup>96</sup> would go on to conclude that cemented “CAD-on” veneers demonstrated higher resistance to fracture than glass fused and manually layered veneers.

In 2015, Renda et al.<sup>12</sup> examined two groups of veneered all-ceramic restorations by measuring the microtensile bond strength between the veneering ceramic and the zirconia framework in the “CAD-on” sample group and a pressed control group. Of note, there was a significant difference between both the mode of failure and the microtensile strength in the two groups. All the samples in the “CAD-on” group underwent adhesive failure, while most of the samples in the pressed group underwent cohesive failure. The difference in failure modes was attributed to the different flexural strengths of the two veneering ceramics. Renda et al.<sup>12</sup> would go on to conclude that microtensile

strengths of the “CAD-on” samples, with a mean strength of 44 MPa, were significantly stronger than the 14 MPa exhibited by the conventionally pressed samples.

In summary, literature published since 2009 suggests that “CAD-on” methodology tends to be more efficient, cost effective, and has higher micotentsile and  $K_{Ic}$  values than conventionally layered all ceramic restorations. The literature also suggests that “CAD-on” restorations are more resistant to veneer fracture in comparison to hand sintered or pressed veneered restorations.

#### **1.4. Testing Methods**

The two adhesive interfaces involving the combination of three ceramic layers consisted of a framework ceramic, an intermediate ceramic, and a veneering ceramic. Fracture or chipping of the veneering structures is a common cause of failure in all-ceramic restorations.<sup>97,98</sup> Ceramics fail primarily because they are brittle, unable to plastically deform, and undergo catastrophic crack propagation.<sup>26</sup> To achieve good long-term performance of a restoration, such as a veneered FDP, the ability of the veneering layer to adhere to the core material is an important factor toward success. According to Anusavice et al. 2013<sup>26</sup>, adhesion can be defined as the attractive intermolecular interactions creating a bond between the boundaries of two materials, while cohesion can be defined as the attractive forces between the molecular constituents within a material. Bond strength can be considered a measure of the adhesive forces between two interfaces and has traditionally been considered an important characteristic and predictor of success of dental restorative materials. Customarily, several mechanical tests have been used to quantify the bond between zirconia and veneering ceramics. For each test, parameters such as dimensions and loading conditions have been prescribed to maintain consistency between studies and within materials. Some common tests investigating the strength of interfaces include the macro and micro

shear bond strength (SBS) tests and the macro and micro tensile bond strength (TBS) tests.<sup>56</sup> Although these tests are relatively inexpensive and easily carried out in dental schools, their results are often inconsistent.<sup>99</sup> A lack of adherence to standardized variables, such as bonding area, storage conditions, ageing of samples, and cross head speeds have been cited as reasons for inconsistency within the dental literature.<sup>100, 101</sup> These inconsistencies have also been associated with variations in stress levels within the tested interfaces.<sup>56, 99</sup> Complex stress patterns are produced when different materials are involved in an adhesive joint. These patterns are unlike a homogeneous material, and are difficult to predict.<sup>56</sup> It has been suggested that mechanical tests that fail to account for complex stress pattern are unreliable and of little use in predicting clinical outcomes.<sup>31, 100-103</sup>

#### **1.4.1. Fracture Mechanics**

According to Hertzberg (1996), fracture mechanics “aims to study and quantify the influence of factors such as stress level, presence of extrinsic and/or intrinsic flaws, inherent materials properties, and mechanisms of catastrophic propagation of a flaw to failure, in order to determine the fracture behavior of a material in aiding future designs.”<sup>104</sup> In brittle materials, flaws and internal defects are randomly distributed throughout the material in irregular shapes and sizes. This random distribution of flaws causes significant variations in strength within a material and within a sample group. Stresses concentrate around inclusions or defects within materials placed under load. A crack begins to propagate uncontrollably and the material fails when the stresses in the area of the defects reach a critical intensity. Depending on the size and location of the defect, unexpected failures in restorative materials can result at stresses well below predicted failure strength. This happens frequently within brittle dental materials such as all ceramic restorations. By examining material behavior and analyzing the effects of stresses and flaws, a fracture

mechanics characterization of dental restorative materials may lead to better predictability of clinical performance.<sup>99,56</sup>

#### **1.4.2. Fracture Toughness**

Each material has a breaking point where the stresses applied to the material cause internal cracks or defects to increase, become critically unstable, and enlarge uncontrollably. By building on the work of Inglis in 1913 and that of Griffith in 1920, and reconsidering the impact of crack shape and the impact of friction, Irwin hypothesized that crack growth is initiated when the energy release rate eclipses the energy required to produce a new crack (Equation 1).

$$\sigma = \sqrt{\frac{EG}{\pi a}}$$

**Equation 1: Irwin's (1957) fracture mechanics formula modification<sup>105</sup>**

Where  $\sigma$  represents the applied stress in the system,  $a$  represents crack length,  $E$  is the modulus of elasticity of the stressed material, and  $G$  is the energy release rate. Irwin established an association between stress, energy release rate, and the materials' modulus of elasticity. By reconfiguring the formula and analyzing crack development, Irwin was able to develop a formula that could describe the stress fields and any point adjacent to the crack tip based on applied loading and the geometry of the structure.

$$\sigma_{ij} = \frac{K}{(2\pi r)^{1/2}} f_{ij}(\theta)$$

**Equation 2: Irwin's introduction of the stress intensity factor equation<sup>56</sup>**

In the above formula (Equation 2), Irwin introduced the concept of a stress intensity factor (**K**). A factor which he hypothesized represented the overall stress field located immediately adjacent to an internal flaw or crack tip when a specimen was loaded under tension. Depending on the angle of force applied, it is possible to load a material in three different load conditions, or modes expressed in Equation 3. Mode I is opening, or tensile mode, where the surfaces of the crack move away from one another; Mode II is a sliding mode, where the surfaces of the crack slide past each other; and Mode III is a torsion mode, where the surfaces of the crack move parallel to each other and match the direction of crack. The stress intensity under each mode of loading is measurable and can be denoted as:

$$\text{Mode I: } K_I = (\sigma_{yy})_L (a\pi)^{1/2}$$

$$\text{Mode II: } K_{II} = (\sigma_{xy})_L (a\pi)^{1/2}$$

$$\text{Mode III: } K_{III} = (\sigma_{zy})_L (a\pi)^{1/2}$$

**Equation 3: Stress intensity factor formulas for three direct types (modes) of loading<sup>56</sup>**

The stress intensity is directly related to the amount of stress applied to the material which is affected by several variables, including the size and shape of the internal defect, and the angle of the force in relation to a defect. The magnitude of K uniquely defines the stress field around the

crack tip for a material. The intensity at which the stress field leads to uncontrollable crack propagation is denoted as  $K_C$ . The critical point where the stress induces crack instability in mode I is  $K_{IC}$ , where I denotes mode I loading and C signifies a critical stress. Equation 4A represents this dynamic relationship for plane stress in very thin objects while Equation 4B illustrates the relationship for plane strain in thicker objects.

$$K_{IC} = \sqrt{EG_{IC}}$$

$$K_{IC} = \sqrt{\frac{EG_{IC}}{1-\nu^2}}$$

**Equation 4 A & B:  $K_{IC}$  formulas with modulus of elasticity E and energy release rate for a plane stress and plane strain condition<sup>105</sup>**

As seen in Equation 4,  $K_{IC}$  incorporates the elastic modulus of the material, making it unique to the tested material and a measurable material property. This measurement has been termed  $K_{IC}$ , and is defined as an intrinsic material property used to characterize the ability of a material to resist unstable crack propagation, caused by internal flaws, under an applied force.<sup>31</sup> Several authors have suggested that the intrinsic component of this measurement makes it material dependent rather than test dependent, and a more suitable test method for assessing dental biomaterials.<sup>56, 105</sup>

### **1.4.3. Fracture Toughness Testing**

As an intrinsic material property,  $K_{IC}$  appears to hold promise in being a reliable quantitative method of comparing the ability of different materials to resist brittle fracture.  $K_{IC}$  has been measured for most restorative materials in dentistry. Some of these materials include amalgam,

denture acrylic, composites, and various ceramics.<sup>26</sup> To achieve reproducibility,  $K_{IC}$  tests have been developed and standardized with strict parameters guiding test protocols. These parameters are the subject of several internationally recognized standards and help enable investigators to accurately compare test results. Some of these tests include the chevron notched short rod (CNSR) specimen  $K_{IC}$  test, the indentation  $K_{IC}$  test, the single edged notched beam (SENB)  $K_{IC}$  test, and the four-point bend specimen  $K_{IC}$  test.<sup>56,99,105</sup> Of note, there have been several examples where different  $K_{IC}$  testing protocols were not able to reproduce the same values or rankings between materials. Irregularities between tests would indicate that some of the testing protocols were improperly conducted or inaccurate.<sup>106, 107</sup> The application of fracture mechanic methodology may provide results that have a better correlation or predictability, with clinical performance.

#### **1.4.3.1. Notchless Triangular Prism Specimen Fracture Toughness Test**

Introduced by Baker et al.<sup>108</sup>, the CNSR specimen  $K_{IC}$  test is a widely used fracture toughness testing method. Sample preparation involves cutting a chevron notch within a cylindrical or rectangular specimen. During tensile loading, crack initiation is intended to take place at the tip of the chevron notch. The production of CNSR samples, specifically the chevron component, has proven to be technically demanding.

In an attempt to simplify sample preparation and improve consistency, Ruse et al.<sup>109</sup> developed the notchless triangular prism (NTP) specimen  $K_{IC}$  test. This test was developed to retain the overall geometry of the CNSR  $K_{IC}$  test while avoiding the production difficulties associated with the production of the chevron notch. Ruse et al.<sup>109</sup> utilized a 6X6X6X12mm triangular prism (Figure 7A), a specimen that could be easily obtained by grinding, casting, or machining.<sup>109</sup>

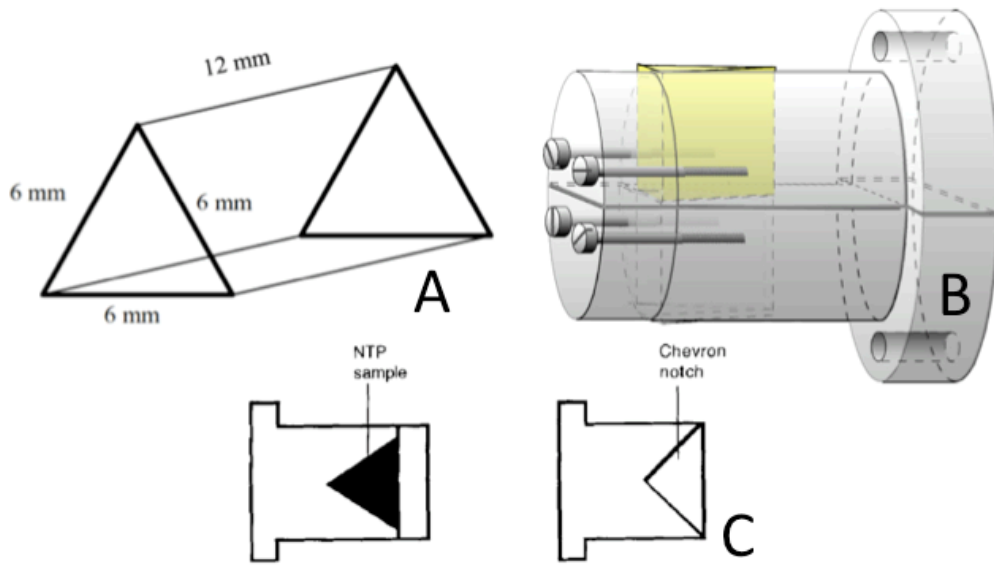


**Figure 7: Notchless Triangular Prism specimen  $K_{IC}$  Test<sup>46, 56, 109</sup>**

- A) NTP sample and dimensions
- B) NTP sample holder with sample
- C) Cross sectional view of NTP sample and sample holder with chevron notch

When fitted into a special specimen holder (Figure 7B), the triangular prism reproduces the chevron shape (Figure 7C) and stress field produced in the CNSR  $K_{IC}$  test. The mounting apparatus consists of a specimen holder, mounting block, spacer blade, and custom designed grips (Figure 25, p.53). The triangular prism is fastened into each half of the specimen holder in a manner that bridges the two halves of the holder. The distance between the two halves of the holder is determined by a spacer blade and is 200  $\mu\text{m}$ . A defect of  $\sim 100 \mu\text{m}$  in depth, to act as a crack initiation point, is introduced into the edge of the prism at the area of the desired stress concentration. The entire specimen holder is secured in the custom designed grips and placed under tensile load at a crosshead speed of 0.1 mm/min in a universal testing machine. By using the same shape and mode of fracture, the calculation of  $K_{IC}$  is based on the original CNSR formula developed

by Bubsey et al.<sup>110</sup> (Equation 5). The value of  $K_{IC}$  is calculated using the original formula where  $P_{max}$  is the maximum load before fracture,  $D$  is the diameter of the test sample (12 mm),  $W$  is the length of the sample (10.4 mm), and  $Y_{min}^*$  is the minimum value of dimensionless stress intensity factor coefficient.

$$K_{IC} = Y_{min}^* \frac{P_{max}}{DW^{1/2}}$$

**Equation 5:  $K_{IC}$  formula used by the CNSR and NTP fracture toughness tests<sup>109</sup>**

In order to determine  $Y_{min}^*$ , Ruse et al.<sup>109</sup> extrapolated known values to accommodate the smaller NTP specimen length to diameter ratios. By plotting Bubsey's experimental data, Ruse et al.<sup>109</sup> extrapolated the NTP  $Y_{min}^*$  to a value of 28. After extrapolation, test results using Equation 5 and the newly calculated dimensionless stress intensity factor coefficient were corroborated by finite element analysis and results on poly (methyl methacrylate). In the finite elemental analysis, stress distributions and magnitudes correlated closely between the NTP and the CNSR. Since its introduction, several other investigations have successfully utilized the NTP specimen  $K_{IC}$  test to determine  $K_{IC}$  of many dental materials. Soderholm et al.<sup>56</sup> praised the simplicity of the NTP approach and suggested that the NTP test had the greatest potential among the standardized  $K_{IC}$  test for more consistency among results.

## Chapter 2: Specific Aim

The aim of this thesis was to apply fracture mechanics methodology and fractography to characterize the adhesive interfaces within the LS2, CC and Y-TZP glass fusion complex produced in the “CAD-on” technique. The interfaces consisted of Y-TZP fused to CC, LS2 fused with CC, and a CAD-on complex of LS2, CC, and Y-TZP. The determined values were compared to the interfacial  $K_{IC}$  of a Y-TZP control veneered with e.max Ceram to establish if “CAD-on” crowns are more resistant to fracture and have the potential for improved intra oral performance. The second aim was to use scanning electron microscopy (SEM) fractographic analysis of representative fractured samples from each group to characterize the fractured surfaces and establish the mode of failure.

### 2.1. Null Hypothesis

The following null hypotheses were tested:

**H<sub>01</sub>:** *There is no significant difference between the interfacial  $K_{IC}$  values for the glass fused LS2 interface and the glass Y-TZP interface.*

**H<sub>02</sub>:** *There is no significant difference between the interfacial  $K_{IC}$  values between the glass fused LS2 and Y-TZP “CAD-on” complex and the Y-TZP pressed veneered control group.*

## Chapter 3: Materials

The materials used in this study are listed in Table 1

Material	Lot	Manufacture and Identification
Lithium disilicate	L54706	IPS e.max CAD (Ivoclar –Vivadent, Liechtenstein)
Yttria stabilized zirconia (Y-TZP)	S48895	IPS e.max ZirCAD (Ivoclar –Vivadent, Liechtenstein)
Glass fusion substrate	T32901	Crystal Connect (Ivoclar –Vivadent, Liechtenstein)
Fluorapatite glass-ceramic veneer	U02631	IPS e.max ZirPress (Ivoclar –Vivadent, Liechtenstein)   LOT
Zirconia conditioner / liner	A34925	IPS e.max Zirliner Ceram Zirliner build-up liquid

**Table 1: Experimental materials**

### 3.1. IPS e.max CAD

IPS e.max CAD (Ivoclar-Vivadent, Liechtenstein) is a proprietary LS2 glass ceramic for CAD/CAM applications, produced in pre-milled ingots (Figure 8). The blocks are initially cast in a controlled heating process where the glass is devitrified to 40% lithium metasilicate crystals.<sup>22</sup>



**Figure 8: IPS emax CAD**

In the lithium metasilicate state, the ingots are blue in colour (Figure 8, p.32), weaker than fully crystallized LS<sub>2</sub>, but durable enough to ensure edge stability during milling. The partially crystallized state remains millable enough for CAD/CAM milling machines, which reduces milling time and limits wear on the milling burs. After milling, the prepared restorations are heat treated to a temperature of 840°C to complete the final step of crystallization.<sup>7, 22</sup> In its final state, the material is composed of 70% LS<sub>2</sub> with a reported flexural strength between 360 – 400 MPa<sup>26, 111</sup> and a K<sub>IC</sub> ranging between 1.9 - 3.3 MPa·m<sup>1/2</sup>.<sup>26, 46</sup> The composition of IPS e.max CAD in its pre-crystallized state, shown in Figure 9A, and is outlined in Table 2. Figure 9B depicts LS<sub>2</sub> after crystallization.

Constituent	Percentage by wt
Silicon dioxide	57 – 80 %
Lithium oxide	11.0 – 19.0 %
Potassium oxide	0.0 – 13.0 %
Phosphorus pentoxide	0.0 – 11.0 %
Zirconium dioxide	0.0 – 8.0 %
Zinc oxide	0.0 – 8.0 %
Colouring oxides	0.0 – 12.0 %

**Table 2: Composition of IPS e.max CAD<sup>22</sup>**

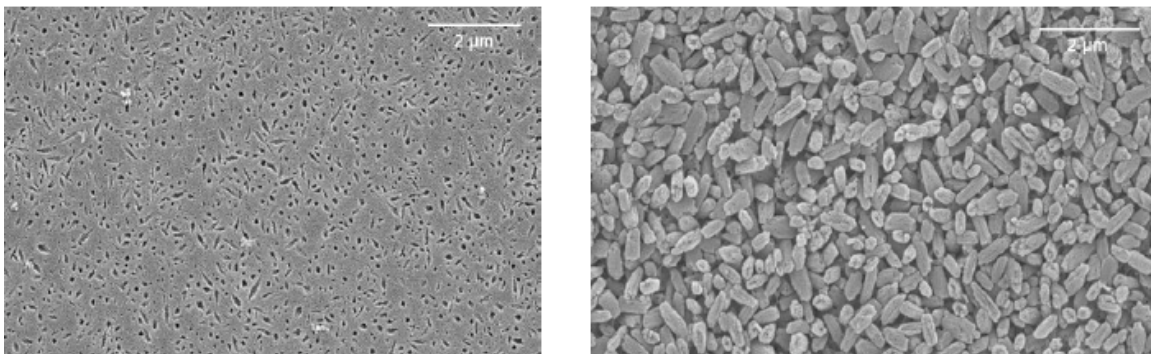


**Figure 9: IPS e.max partially and fully crystallized states<sup>3</sup>**

### 3.2. IPS e.max ZirCAD

The makeup of the pre-sintered ZirCAD ingot (Figure 10) is very porous, at roughly 50%, with the grains of the structure only weakly connected to one another. The manufacturer describes these connections as weak sintering necks that are formed during the pre-sintering ingot fabrication process.<sup>112</sup> The porosity and pre-sintering connections make the strength of the material sufficiently low to facilitate ingot reduction and reduce maintenance costs of the milling device.

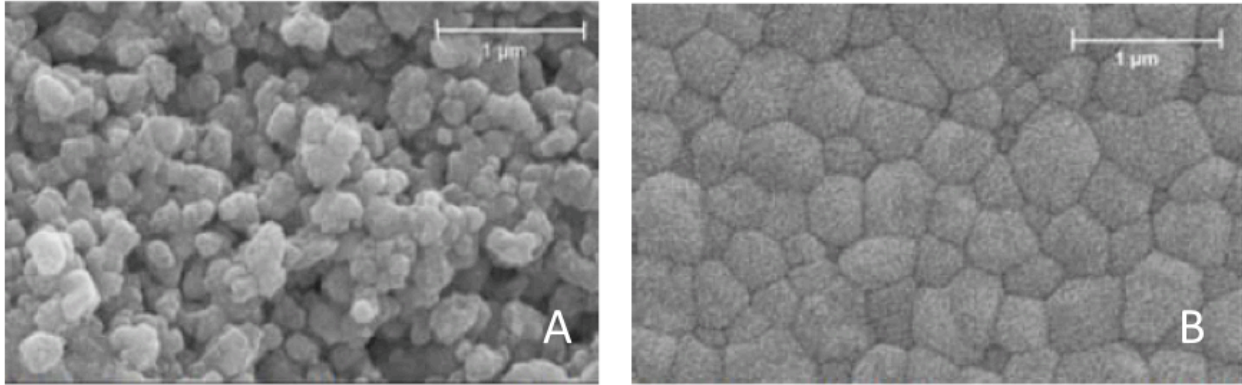


Figure 10: IPS e.max ZirCAD<sup>112</sup>

After ingot reduction, the material is sintered to strengthen it, a process that condenses its internal crystalline structure and converts the remaining grains to a tetragonal structure (Figure 11, p.35). The final volume of the restoration decreases by 20 – 25% of the pre-sintered milled restoration.<sup>22</sup>

<sup>112</sup> Fully sintered ZirCAD restorations have flexural strengths ranging between (900 – 1200) MPa

<sup>28</sup> and  $K_{IC}$  ranging between (4.8 - 7.7)  $\text{MPa}\cdot\text{m}^{1/2}$ .<sup>70, 71</sup>



**Figure 11: Microstructure of (a) presintered and (b) sintered IPS e.max Zir CAD<sup>22,112</sup>**

The composition of IPS e.max CAD in its pre-crystallized state, as listed by the manufacturer, is contained in Table 3 (p.35).

<b>Constituent</b>	<b>Percentage by WT</b>
Zircon dioxide	87 – 95.0 %
Yttrium oxide	4.0 – 6.0 %.
Hafnium oxide	1.0 – 5.0 %
Aluminum oxide	0.0 – 1.0 %

**Table 3: Composition of IPS e.max ZirCAD<sup>22</sup>**

### **3.3. Crystal Connect™**

IPS e.max CAD is a fluorapatite glass-ceramic fusing material used in the IPS e.max “CAD-on” technique. At approximately 840°C, simultaneous sintering of the connecting glass and crystallization temperature of the e.max CAD creates a “homogeneous bond” between the veneer, the connecting glass, and the ZirCAD framework.<sup>22, 113</sup> With the exception of the approximate percentages of its constituents, very little is known about the physical characteristics of the connecting glass. According to the manufacturer, CC consists of SiO<sub>2</sub> (50%), Al<sub>2</sub>O<sub>3</sub> (8–22%),

Na<sub>2</sub>O (6– 10%), K<sub>2</sub>O (4-8%), and ZnO (1–3%).<sup>22</sup> An extremely high moisture content allows the pre-sintered CC to behave as a thixotropic solid, permitting the spread of the glass intermediate between the veneer and the framework during production.<sup>22, 113</sup>

### 3.4. IPS e.max ZirPress

The manufacturer of IPS e.max ZirPress identifies ZirPress as a suitable material to be pressed over IPS e.max ZirCAD single-tooth and multi-unit bridge Y-TZP abutments and frameworks. ZirPress is a glass-ceramic ingot (Figure 12, p.36) that contains fluoroapatite crystals Ca<sub>10</sub>(PO<sub>4</sub>)<sub>6</sub>F<sub>2</sub>. The crystals range in size from 300 nm in length and roughly 100 nm in diameter. Its composition, as provided by the manufacturer, is listed in Table 4 (p.37).

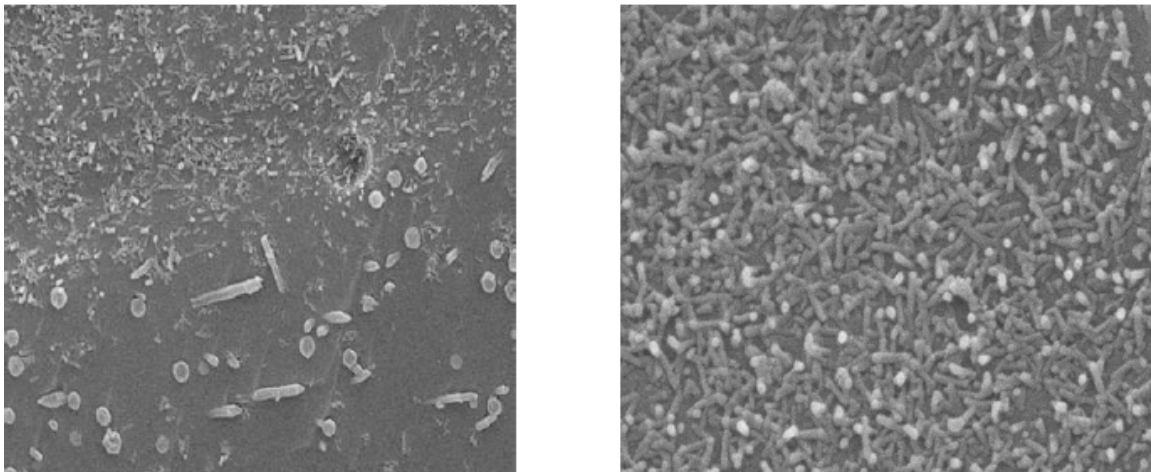


Figure 12: IPS e.max ZirPress ingot

Constituent	ZirPress	ZirLiner
Silicon dioxide	57 – 63 %	50 – 60 %
Aluminum oxide	12.0 – 16.0 %	16 – 22 %
Sodium Oxide	6.0 – 8.0 %	6 – 11 %
Potassium oxide	2.0 – 4.0 %	4 – 8 %
Zirconium dioxide	1.5 – 2.5 %	2.0 – 4.0 %
Phosphorus pentoxide	1.0 – 2.0 %	2.5 – 7.5 %
Fluorine	0.5 – 1.0 %	N / A
Other oxides and pigments	0.2 – 0.9 %	0.1 – 3.0 %

**Table 4: Composition of IPS e.max ZirPress and IPS e.amx ZirLiner.<sup>74</sup>**

According to the manufacturer, the fluoroapatite crystals impart opalescence to restorations manufactured with ZirPress. The fluoroapatite crystals incorporated into the veneering layer differ in size and shape (Figure 13).



**Figure 13: Variation of crystal size within IPS e.max ZirPress<sup>74</sup>**

The ZirPress ceramic ingot is pressed onto zirconium oxide via a lost wax press-over technique. Several recent clinical trials have been completed involving restorations veneered using IPS e.max Zirpress.<sup>114, 115, 116, 117</sup> Each of these trials ranging from 3 - 5 years in length involved ZirPress and

zirconia frameworks. Together, these trials totalled over 175 ZirCAD copings and 78 ZirCAD multi-unit frameworks with clinical success rates ranging from (88.2 - 95.7)%. Flexural strength of the veneered complex ranged between (89.0 – 110.0) MPa<sup>55, 79</sup>. Microtensile strength of the combined veneer zirconia framework was cited as 14.9 MPa, considerably lower than the CAD-on veneer examined in the same investigation.<sup>12</sup>

### **3.5. ZirLiner**

ZirLiner ceramic is a semi translucent apatite glass that is similar in composition to ZirPress but contains slightly more zirconium oxide. It is used to prime the surface of the Y-TZP in preparation for ZirPress application. According to the manufacturer, ZirLiner is used to obtain a “sound bond” between the framework and the apatite glass veneering material.<sup>74</sup> ZirLiner is also used to adjust the shade and translucency of the restoration by adapting the thickness of each application. The composition of ZirLiner as provided by the manufacturer is listed in Table 4 (p.37).

## Chapter 4: Methods

### 4.1. Sample Size Calculation

Lehr's sample size equation (Equation 6)<sup>118</sup> was used in a power calculation to determine sample size. A study by Della Bonna et al.<sup>119</sup> was used as a pilot study for the calculation of the standardized difference. A 20 % difference between means was considered of clinical significance.

#### Rule of Thumb

The basic formula is

$$n = \frac{16}{\Delta^2},$$

where

$$\Delta = \frac{\mu_0 - \mu_1}{\sigma} = \frac{\delta}{\sigma}$$

**Equation 6: Lehr's basic Rule of Thumb equation<sup>118</sup>**

In the above equation,  $\Delta$  is the standardized difference,  $\delta$  the treatment difference and  $\sigma$  the standard deviation. With a standardized difference calculated to be 1.13, at 95 % confidence level, and power of 80 %,  $n$  was calculated to be 14 samples per test group.

Considering the brittle nature and the predicted flaw distribution within ceramic materials, Weibull statistics was used to analyze the results. The probability  $P$  that a ceramic material will fracture at a given stress can be estimated by the formula found in Equation 7.<sup>120, 121</sup>

$$P = 1 - \exp \left[ - \left( \frac{x}{x_0} \right)^m \right]$$

**Equation 7: Fracture probability of a ceramic<sup>120, 121</sup>**

Studies by Tiryakioglu et al.<sup>120</sup>, Langlois et al.<sup>121</sup> and others have determined that group sizes with a sample population with at least 20 samples produce less bias when utilizing Weibull statistics. For this reason, as well as the possibility of processing flaws, it was decided that each test group target size would be 22 samples.

## 4.2. Experimental Design

The experimental design is summarized in Table 5.

Material	Group	Tested Property	Sample (n)
LS2 CAD – glass interface	I	Interfacial $K_{IC}$	22
Y-TZP CAD – glass interface	II	Interfacial $K_{IC}$	22
YTZP CAD – glass – LS2 interface	III	Interfacial $K_{IC}$	22
Y-TZP – e.max ZirPress	IV	Interfacial $K_{IC}$	22

**Table 5: Experimental design**

Test group I was designed to isolate LS2’s interaction with CC without the possible interference of Y-TZP. Similarly, group II was designed to isolate the interaction of Y-TZP with CC. Measuring and comparing the interfacial  $K_{IC}$  of group I and group II would isolate both sides of the failed CC interface and allow for a thorough examination of the interfaces, measurement of interfacial  $K_{IC}$  values for the two different adhesive interfaces, and testing of the first null hypothesis ( $H_{01}$ ). Group III was designed to evaluate the entire “CAD-on” junction of the LS2, CC, and Y-TZP complex. Group IV was the control group representing a conventionally pressed fixed restoration. Measuring and comparing test group III and IV would allow for a direct

comparison between the “CAD-on” technique and a conventionally pressed control. It also tests the second null hypothesis ( $H_{02}$ ).

### **4.3. Sample Preparation**

As outlined in Table 5 (p.40), 4 groups of 22 NTP specimens (6X6X6X12 mm) were produced. Initially, 9 IPS Emax CAD blocks (LS2), and 11 IPS Emax ZirCAD blocks (Y-TZP) were divided to produce quarter sections as illustrated in Figure 15 (p.42). In total, 36 LS2 and 48 Y-TZP quarter sections were produced. Each IPS e.max CAD block quarter section was ground to a 6X6X6X12 mm triangular prism as shown in Figure 16 A, B, and C (p.43). Each e.max ZirCAD quarter section was ground to an oversized 8X8X8X19 mm triangular prism to account for 20-25 % shrinkage during sintering. The oversized Y-TZP sections were then sintered according to manufacturer firing protocol and refined to the desired 6X6X6X12 mm triangular prism size. After each of the quarter section prisms were refined to the correct size, the long prisms were sectioned in half, as shown in Figure 16 D (p.43), to produce half prisms. In total, 72 6X6X6X6 mm half LS2 prisms were produced, and 96 6X6X6X6 mm half Y-TZP prisms were produced. To illustrate, the fabrication of a LS2 half-sample is outlined in Figures 15, 16, 17, and 18 (pp.42-4). Sectioning of all blocks was carried out with the use of an Isomet low speed saw (Buehler, Lake Bluff IL) and diamond impregnated slicing wheels (UKAM, Valencia, CA) under continuous water irrigation (Figure 14).



**Figure 14: Low speed Isomet saw**

The first step of fabrication of the LS2 half-samples was the removal of the metal milling stem from each IPS e.max block by sectioning. Each stemless ingot was then sectioned into four (14x12.5x8) mm cuboid blocks (Figure 15).

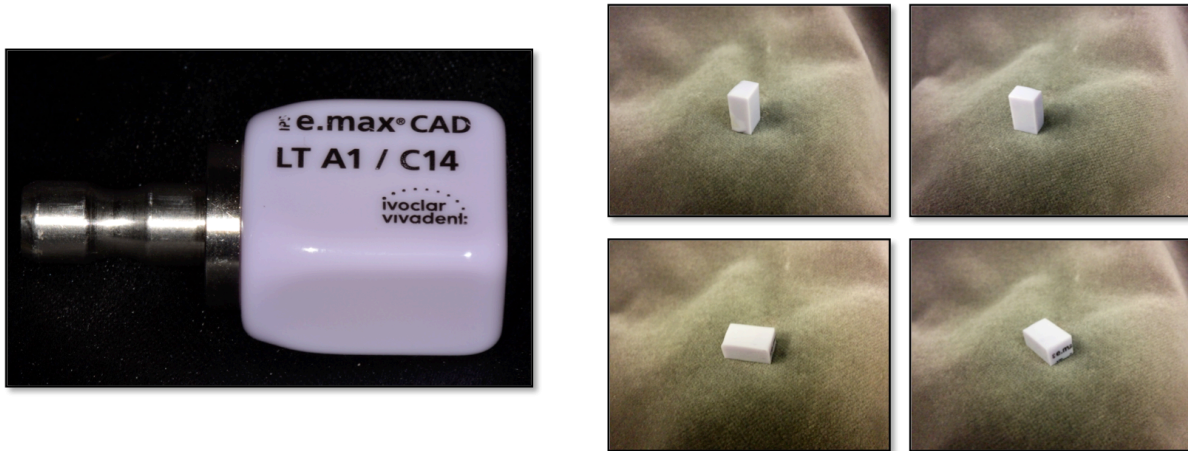


**Figure 15: Cutting steps of IPS e.max CAD NTP half specimens**

The cuboid blocks were marked with an outline of the prism (Figure 16 A) and ground into 6X6X6X12 mm prisms using a custom grinding jig and 120 grit SiC paper discs (Buehler, Lake Bluff, IL) (Figure 16 B&C). Each 6X6X6X12 mm prism was then sectioned mid-length to produce two half prisms (Figure 16 D).

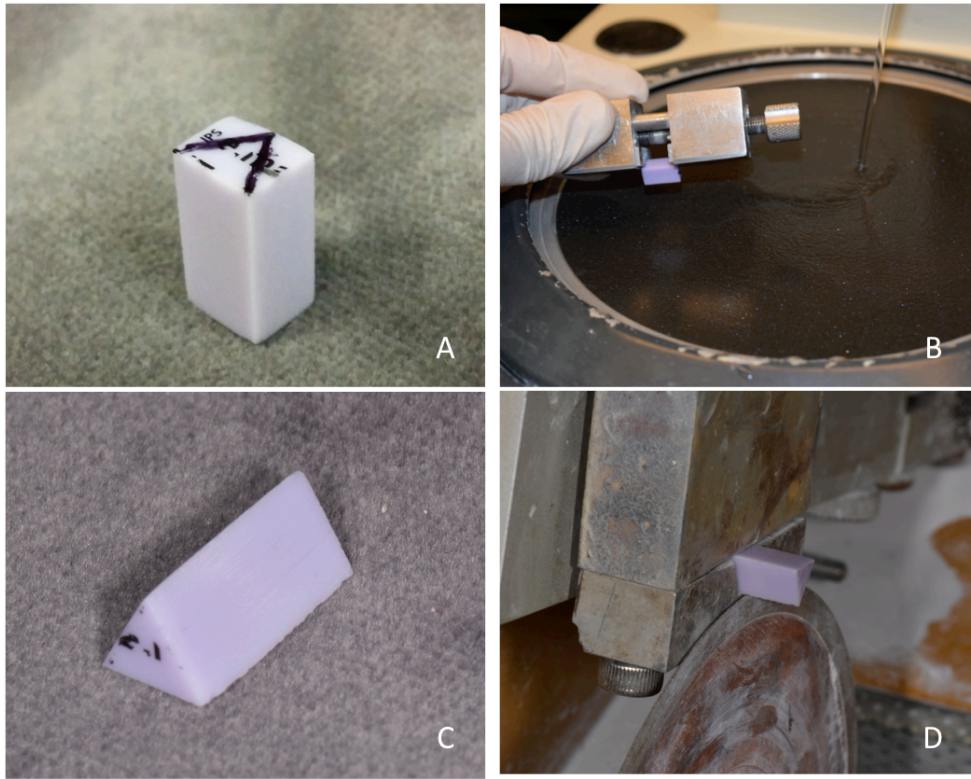


**Figure 16: Grinding and section steps of the IPS e.max CAD half specimen**

#### **4.4.Alignment and Glass Fusion (Test Groups)**

Depending on the test group, two half specimens were approximated, with the correct fusion counterpart, inside an alignment jig (Figure 17 B, p.44). Under high frequency vibration, the thixotropic CC solid substrate was converted to a liquid form and used to lute half specimens together to create a complete 6X6X6X12 mm specimen, corresponding to groups A, B, or C (Figure 17 A – D, p.44). After approximation, a finger spring was used to maintain alignment

while transferring the assembled sample from the aligning jig to the oven for crystallization (Figure 17 E, F).

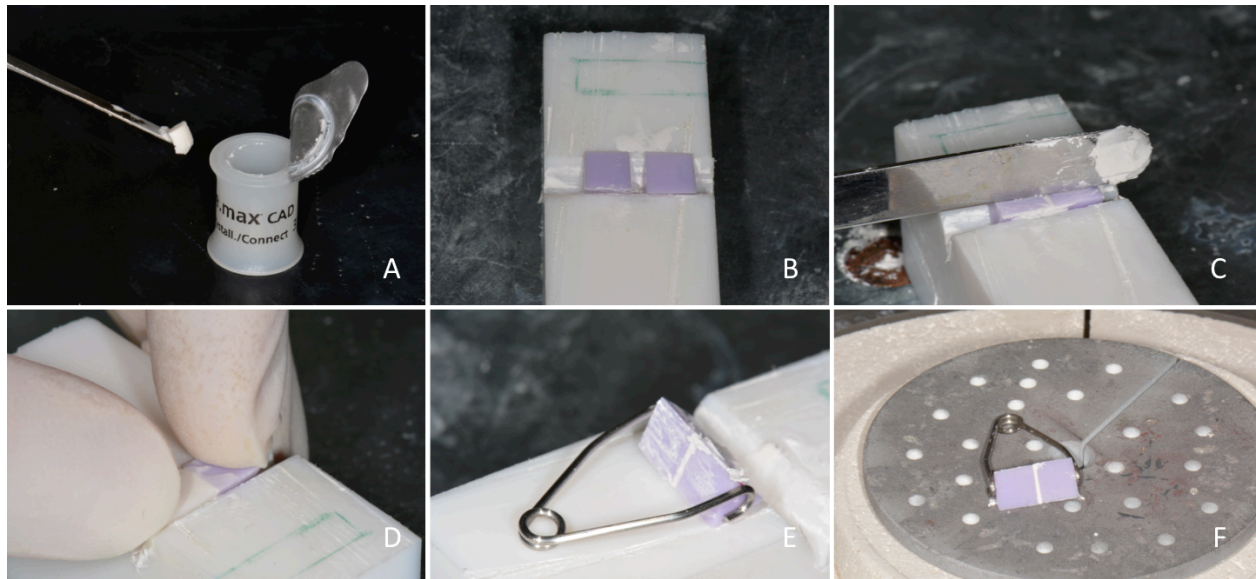


**Figure 17: Alignment and luting of the NTP test half specimens**

The assembled specimens were fired in a Programet 500 oven at 840 °C, where the LS2 and CC components were fully crystallized and simultaneously fused with their corresponding half samples (Figure 18 A & B, p.45). The 86 ZirCAD half samples, which required a longer firing cycle at 1500 °C, were sintered prior to the alignment and luting phase.

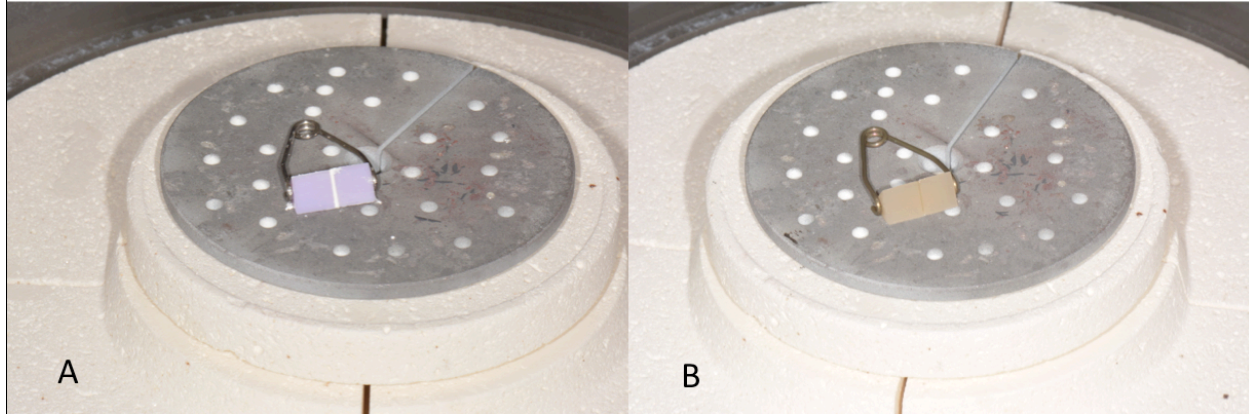


**Figure 18: Glass fusion and crystallization of an LS2 – CC – LS2 NTP test specimens (A) Before crystallization (B) After crystallization**

After cooling, the test samples were polished and refined with 600 grit SiC paper discs (Buehler, Lake Bluff, IL) to exact dimensions prior to fracturing.

#### **4.5. Control Sample Production**

According to manufacturer instructions, the adhesive surface of each control half-sample Y-TZP NTP prism was coated with ZirLiner (Figure 19 D, p.46). The application of ZirLiner involved the steaming of each surface (Figure 19 C, p.46) prior to the application of a slurry, consisting of ZirLiner build-up liquid and ZirLiner powder, as illustrated in Figure 19 A, B, & D (p.46).

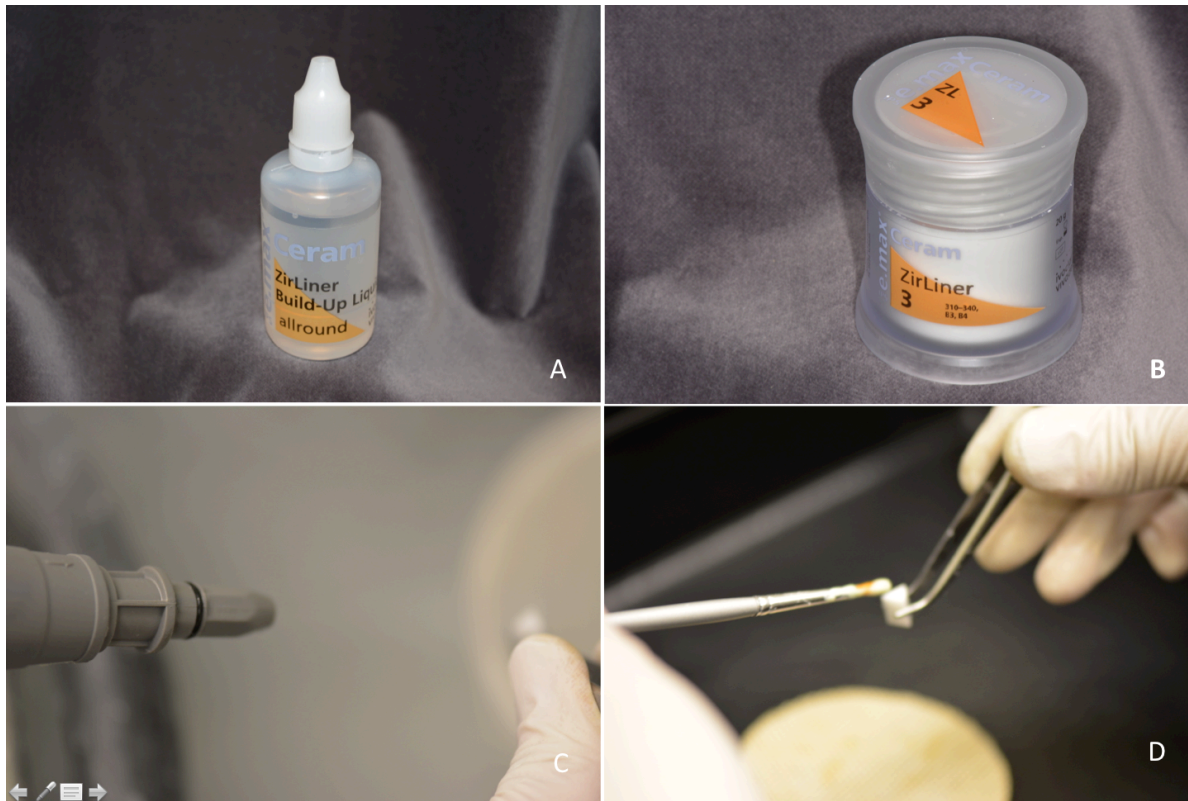


**Figure 19: IPS e.max ZirLiner materials and application**

After the application of ZirLiner, the wax-up ZirPress portion of each control sample was fabricated. To produce wax-ups with the correct dimensions, an ideal poly (methyl methacrylate) replicate template was produced. A mould of the template was manufactured by investing the template prism in heavy body polyvinylsiloxane bite registration material (Aquasil, Dentsply, York, PA) (Figure 20 C, p.47). The template was designed longer than the standard 12 mm prism (6X6X6X15 mm) to accommodate the Y-ZTP component, a thin ZirLiner application, and the proper amount of molten dipping wax (Whip Mix, Louisville, KY). An image of the disassembled and assembled five-piece mould and a control sample are shown in Figure 20 A, B, & C (p.47). A completed waxed control sampled is shown in Figure 20 D (p.47).

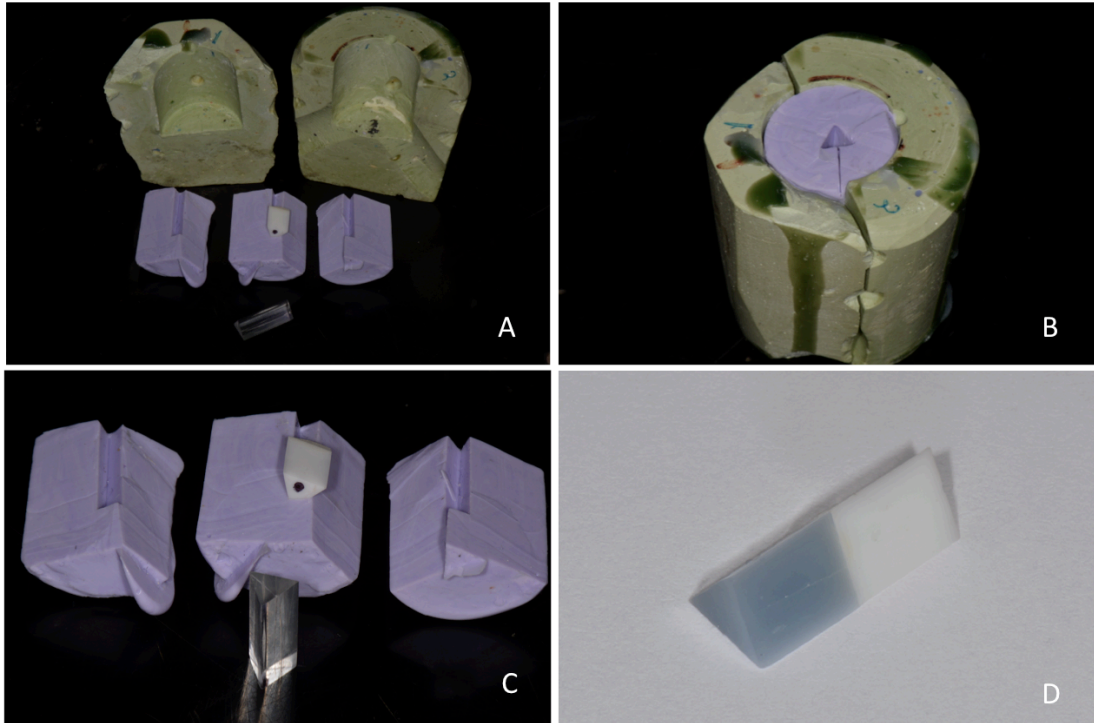


**Figure 20: IPS e.max ZirPress wax mould with ZirCAD half specimen and clear template disassembled mould. (D) Assembled wax mould**

The ZirPress components were pressed at the Ivoclar-Vivadent research facility (Buffalo, NY). Each of the wax-up control samples was sprued prior to investment and pressing. Wire wax (ABF-wax, Metalor, Canada), as illustrated in Figure 22 A (p.49), was used to connect the wax-up end of each sample to an Ivoclar ZirPress investment ring (Figure 22 B, C, D, p.49). The IPS investment ring system was used according to the manufacturer's standards, as outlined in Figure 21 (p.48).

	Single-Tooth Restorations	Bridges
Investment Ring System	100 g, 200 g, 300 g	200 g, 300 g
Diameter of the wax wire	3 mm	3 mm
Length of the wax wire	min. 3 mm, max. 8 mm	min. 3 mm, max. 8 mm
Length of the wax wire including waxed-up object	max. 16 mm (100 g, 200 g) max. 20 mm (300 g)	max. 16 mm (200 g,) max. 20 mm (300 g)
Sprue attachment point at the waxed-up object	thickest part of the wax-up	bridge abutments and each bridge pontic
Sprue angle to the waxed-up object	axial	axial
Sprue angle to the ring base	45–60°	45–60°
Design of the attachment points	round and slightly tapered, no sharp angles or edges	round and slightly tapered, no sharp angles or edges
Distance between the objects and the sprues	min. 3 mm	min. 3 mm
Distance to the silicone ring	min. 10 mm (check with the IPS Sprue Guide)	min. 10 mm (check with the IPS Sprue Guide)
Note		Larger bridges may also be placed in the center of the investment ring.

**Figure 21: ZirPress sprueing guidelines** <sup>74</sup>

No more than four samples were sprued to a ring. Each ring was invested with a phosphate-bonded investment gypsum (IPS PressVest Speed) as shown in Figure 22 F (p.49).

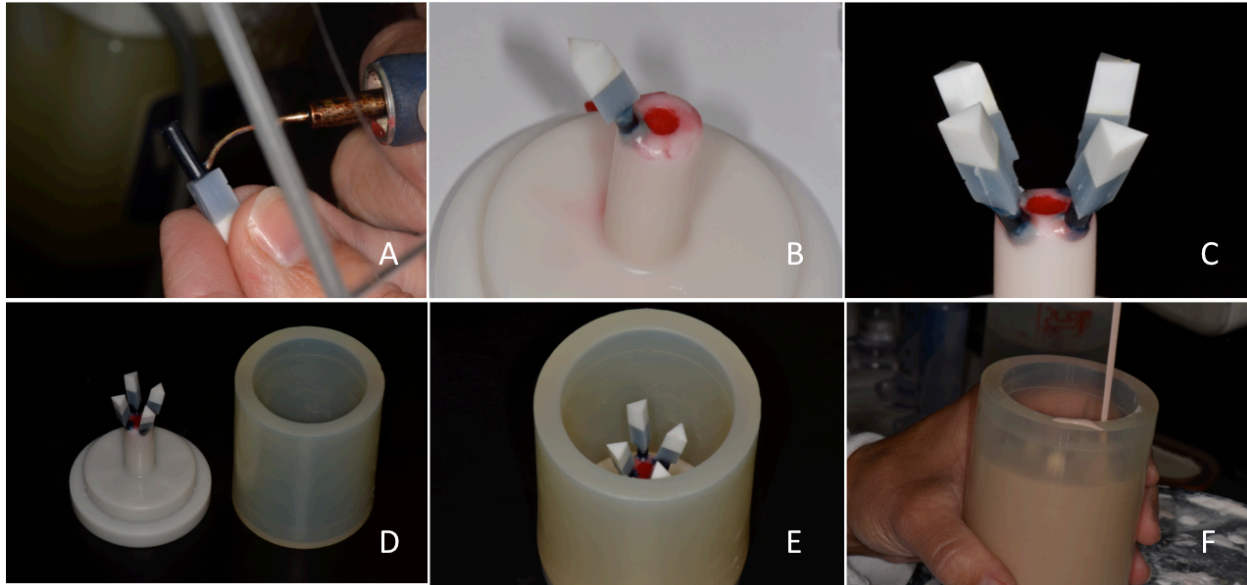


**Figure 22: IPS e.max ZirPress sprueing and investment sequence**

After the required 45 minutes investment medium setting time, the ring gauge and ring base were separated from the investment ring. The rings were then inspected and allowed to stand for an additional 15 minutes (Figure 23 A). Before adding the ZirPress to the investment ring, the investment rings were placed in a preheating oven according to the manufacturer's directions (Figure 23 B). After preheating, three HT C2 ZirPress ingots and an IPS Alox Plunger were added to each of the investment rings. The rings were then inserted into an EP 5000 Programat press oven (Ivoclar – Vivadent, Liechtenstein) and fired through the press cycle (Figure 23 C).



**Figure 23: IPS e.max ZirPress firing and pressing sequence**

<b>Component</b>	<b>Parameter</b>
Press Furnace	Programat EP 5000
IPS investment ring system	High Translucency
IPS investment ring system	300g (IPS PressVest Speed)
Stand-by temperature (°C / °F)	700/1292
Temperature increase (°C / °F / minute)	60 / 108
Holding temperature (°C / °F)	900 / 1652
Holding time (minutes)	15 minutes
Vacuum on (°C / °F)	500 / 932
Vacuum off (°C / °F)	910 / 1670
Long-term cooling	0

**Table 6: Press Parameters for IPS e.max ZirPress**

After cooling for 45 min, the investment material surrounding the sample was broken down using a microblaster (Comco Inc.) with 80  $\mu$ m glass beads at 250 kPa (Figure 24 A&B, p.51). After separation from the investment material, each sample was detached from the sprue and remaining ingot with a rotary handpiece (NSK Ti-Max Z95L, Nakanishi International) (Figure 24 C, p.51) and diamond disk (Brasseler 850 medium, Brassler, USA). After separation, each sample was polished down to accurate dimensions using 120 grit SiC paper discs (Buehler, Lake Bluff, IL) (Figure 24 D, p.51).

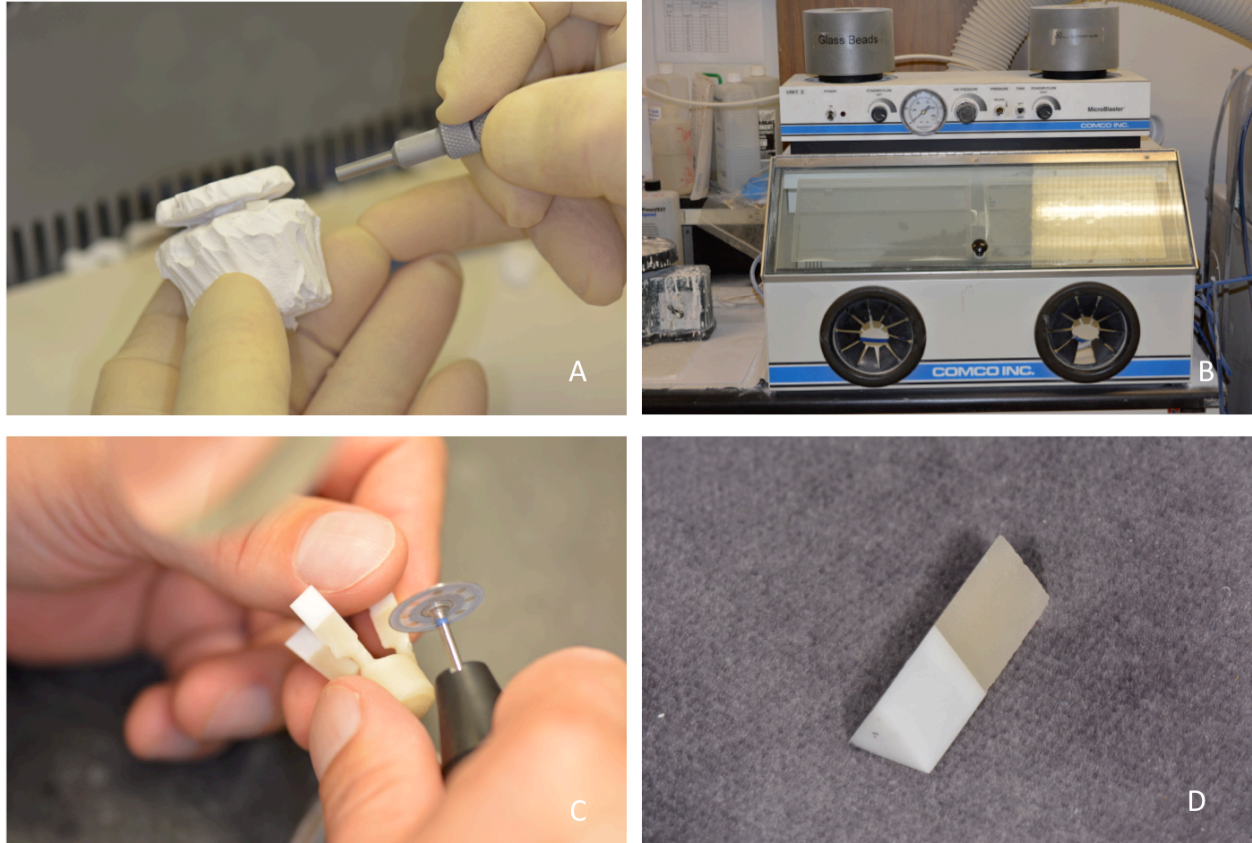


**Figure 24: IPS e.max divestment and finishing sequence**

#### **4.6. Interfacial $K_{IC}$ Determination**

The NTP specimen  $K_{IC}$  test was used to determine the interfacial  $K_{IC}$  for the test samples created in the four groups. A similar sequence of steps was used to load, stress, fracture, and calculate  $K_{IC}$ . Initially, each specimen was loaded into one side of the NTP specimen holder, aligning the bonded interface with the midline of the specimen holder (Figure 25A & B, p.52). Correct alignment of the sample was confirmed under a light microscope. Crack initiation was completed with a 200  $\mu\text{m}$  cutting blade (Figure 25 C, p.52) and verified under a light microscope.

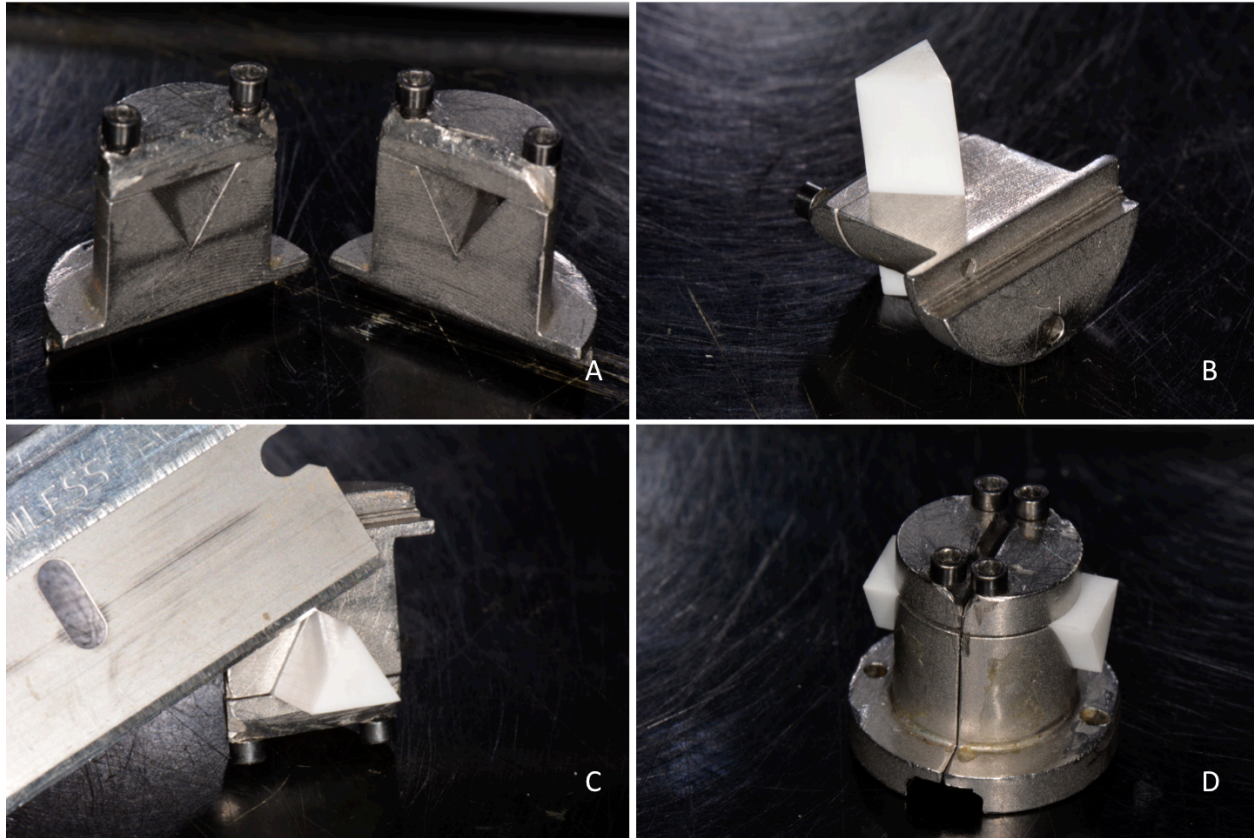


**Figure 25: NTP test sample loading and defect creation**

The cover cap test screws were secured after the test specimen was placed in the specimen holder (Figure 25 D), and a 200  $\mu\text{m}$  thick blade was used to space the assembled specimen correctly in the mounting jig (Figure 26 A, p.53). The specimen holder was loaded, with the use of custom grips, in an Instron 4301 universal testing machine with a 1 kN Instron load cell (Figure 26 B, p.53). The Instron 4301 was computer controlled with BlueHill software. The specimen holder was loaded in tension at a crosshead speed of 0.1 mm/min until crack arrest or sample failure.

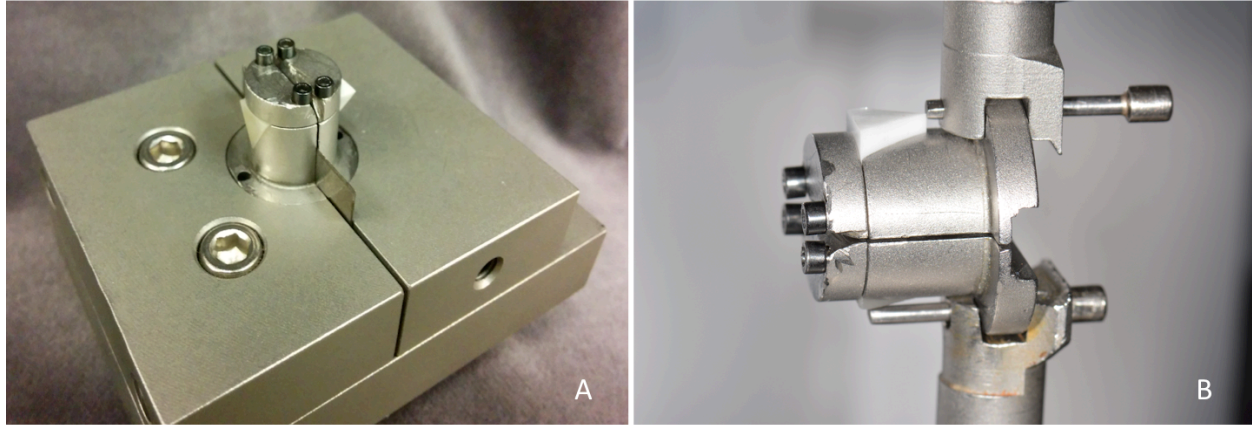


**Figure 26: NTP holder/testing**

- A) NTP specimen holder in mounting block with metal spacer
- B) NTP specimen loading in Instron testing machine

As the tension was applied to the specimen, both the force applied and the displacement were recorded and charted by the BlueHill computer software. The greatest amount of force that was recorded was used in Equation 5 (p.30) to calculate interfacial  $K_{IC}$  values.

#### **4.7. Light Microscopy Investigation**

For each fractured sample, the two halves of the specimen were examined under a light microscope, similar to the setup shown in Figure 27 (p.54). Each half was characterized in terms of surface texture, defects, failure mode, amounts of fusing glass, and the site of crack initiation. All test specimens involving the glass fusion methodology appeared to exhibit cohesive failure. Although most of the interfaces were smooth with approximately equal amounts of CC glass on each of the fracture surfaces, some fractured samples displayed irregular fracture patterns with obvious defects or voids. Interfaces with voids, defects, or roughened surface appeared to correlate with lower interfacial  $K_{IC}$  values. Most of the higher  $K_{IC}$  values appear to be associated with smoother fracture patterns which contained fewer defects.

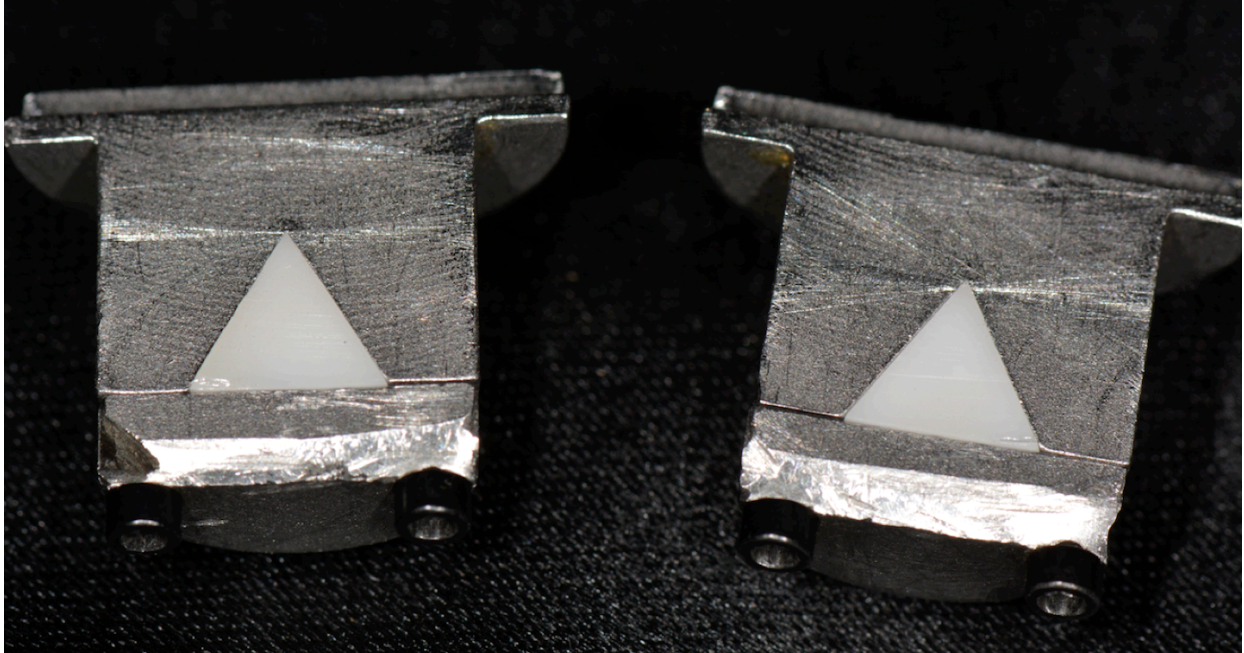


**Figure 27: Specimen holder and fractured samples**

#### **4.8.Scanning Electron Microscopy**

Fractographic analysis, using a scanning electron microscope (SEM), was performed to assist in the characterization of the fracture surfaces. The SEM images were produced by a (Hitachi, S-3000N (Hitachi, Japan) SEM (Figure 28 A, p.55). Four samples from each test group were selected for scanning. Sample selection was based on the amount of force required to fracture. Two samples closest to the average fracture force within each test group were selected. Two additional samples, the lowest and highest force in each test group, were also scanned. Prior to scanning, each fracture surface was gold coated with an Edwards S150A sputter coater (Edwards Vacuum, Crawler, UK) (Figure 28 B, p.55). After coating, the samples were inspected via SEM at several magnifications and micrographs were saved in JPG format.

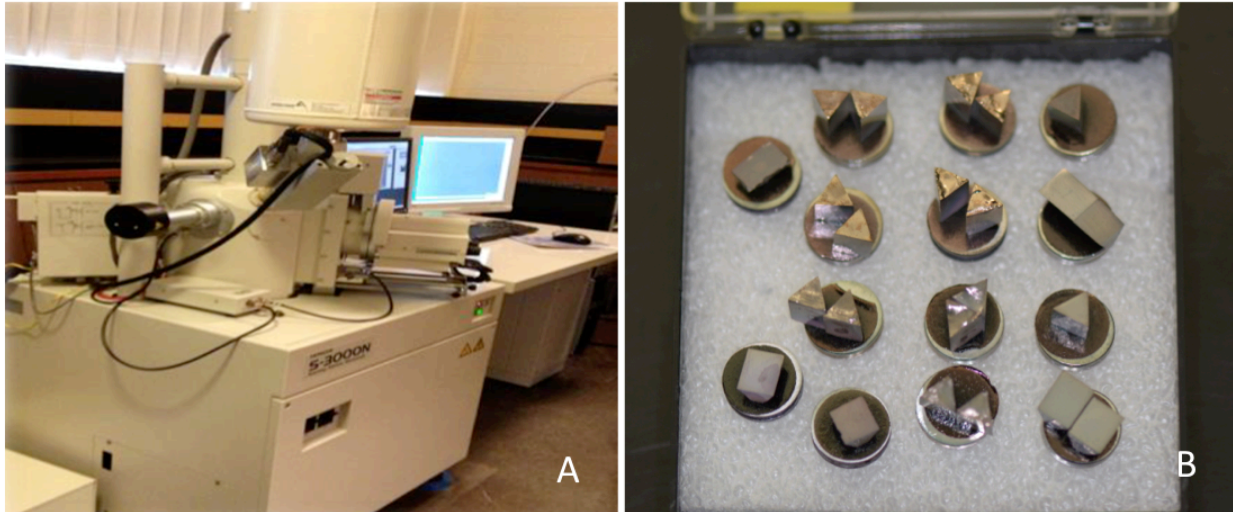


**Figure 28: SEM and SEM samples**

#### **4.9. Statistical Analysis**

The  $K_{IC}$  results were analyzed by Weibull statistics and by one-way **ANOVA** which was followed by Scheffé multiple means comparisons ( $\alpha=0.05$ ), using SPSS (SPSS for Mac, version 23; Chicago, IL) Scheffé test allows for comparisons between multiple groups with uneven numbers, identifying significant differences between multiple groups. In Weibull statistics,  $m$  represents the slope of the measured  $K_{IC}$  and the probability of failure curve. It provides an indication of reliability for each of the tested materials. Equation 8 produces the Weibull parameters in a graphical format, where the slope and reliability can be calculated, allowing for a visually comparison between materials.

$$\ln \left[ \ln \left( \frac{1}{1 - P_f} \right) \right] = m \ln \sigma - m \ln \sigma_0$$

**Equation 8: Weibull formula producing graphic and Weibull modulus**

Steeper slope values represent more reliability. The characteristic Weibull value ( $K_{IC}$ ) was also determined: it is the experimental value corresponding to a probability of failure of the 63.2%.<sup>122</sup>

## Chapter 5: Results

### 5.1. Interfacial $K_{IC}$

Twenty-two samples were prepared for each group. Unfortunately, some samples failed during mounting, resulting in test groups ranging between 16 - 21 samples per group. Although the minimum intended sample size of 22 specimens was not universally obtained, each group still exceeded the minimum required number of specimens as calculated by the Lehr sample size equation (Equation 6, p.39). It is not uncommon in the literature to have Weibull analysis performed on group sizes of 15.<sup>122, 123</sup> Descriptive statistics, which include the mean and standard deviation for the three test groups and the control group, are presented in Table 7.

Material	Group	Group Size	$K_{IC}$ (MPa·m <sup>1/2</sup> ) (Mean ± SD)*
E <sub>max</sub> – CC – E <sub>max</sub>	I	21	1.04 ± 0.26 <sup>a</sup>
Zir – CC – Zir	II	17	0.87 ± 0.16 <sup>ab</sup>
Zir – CC – E <sub>max</sub>	III	19	1.10 ± 0.28 <sup>a</sup>
Zir – L – ZirP (control)	IV	16	0.71 ± 0.08 <sup>b</sup>

Table 7: Test groups and mean  $K_{IC}$

The characteristic Weibull values for each group (Table 8) were calculated using Equation 8 (p.55).

Group	Weibull	
	m	$K_{IC}$
I	4.51	1.13
II	5.16	0.92
III	4.34	1.24
IV	10.45	0.74

**Table 8: Weibull modulus and Weibull  $K_{IC}$**

A one-way ANOVA of the interfacial  $K_{IC}$  revealed that a significant difference existed between the four test groups. The complete results of the Scheffé’s test can be found in Table 9 (p.58). The Scheffé’s test indicated that no significant differences exist between groups I, II and III. Moreover, group three was significantly different from group IV (control). Based on these results the first null hypothesis can be accepted as there does not appear to be a difference between the interfacial fracture  $K_{IC}$  of the Zir – CC interface and the Emax – CC interface. The test also indicated that a significant difference does not exist between groups II and IV. A significant difference between groups III and IV suggests that the “CAD-on” group had a significantly higher interfacial  $K_{IC}$  than the control, thus rejecting the second null hypothesis.

### Multiple Comparisons

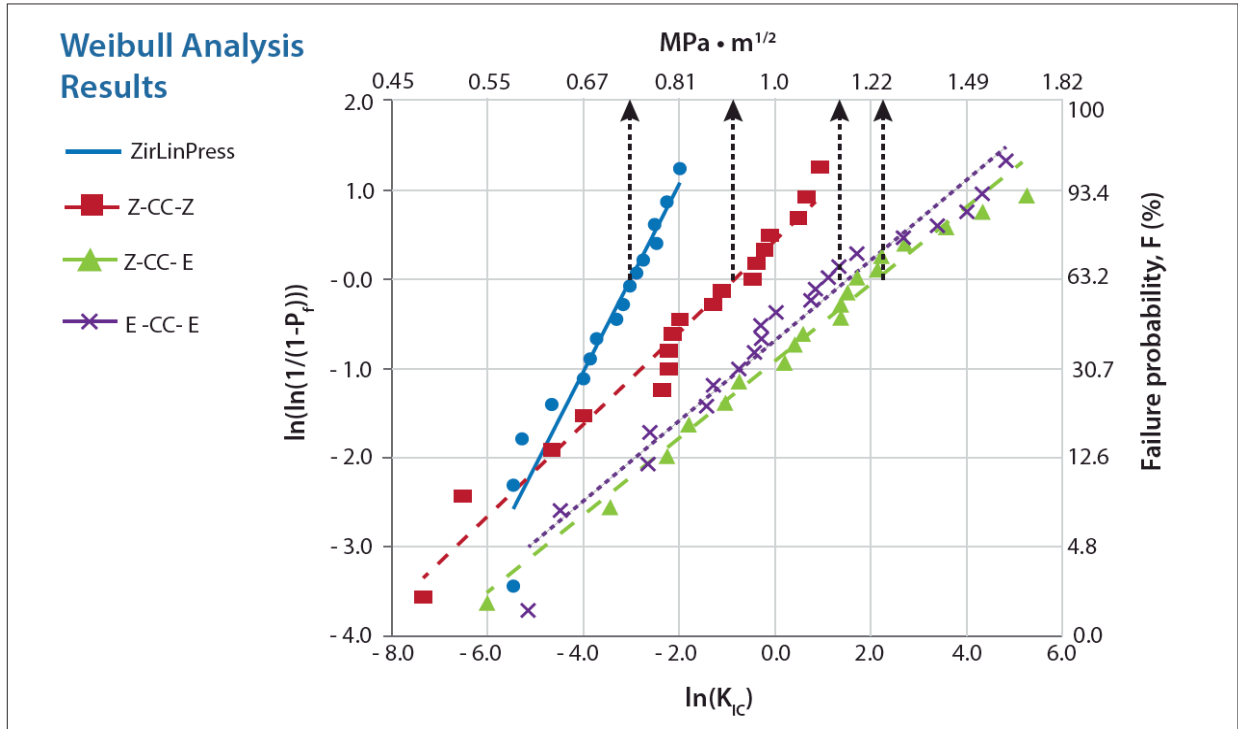
Dependent Variable: KIC  
Scheffe

(I) Group	(J) Group	Mean Difference (I-J)	Std. Error	Sig.	95% Confidence Interval	
					Lower Bound	Upper Bound
EmaxCCT	ZirCTEmax	-.03930	.07073	.958	-.2420	.1634
	ZirCCT	.16745	.07288	.163	-.0414	.3763
	ZirLinP	.35708*	.07413	.000	.1446	.5695
ZirCTEmax	EmaxCCT	.03930	.07073	.958	-.1634	.2420
	ZirCCT	.20675	.07458	.062	-.0070	.4205
	ZirLinP	.39638*	.07580	.000	.1792	.6136
ZirCCT	EmaxCCT	-.16745	.07288	.163	-.3763	.0414
	ZirCTEmax	-.20675	.07458	.062	-.4205	.0070
	ZirLinP	.18963	.07781	.125	-.0333	.4126
ZirLinP	EmaxCCT	-.35708*	.07413	.000	-.5695	-.1446
	ZirCTEmax	-.39638*	.07580	.000	-.6136	-.1792
	ZirCCT	-.18963	.07781	.125	-.4126	.0333

\*. The mean difference is significant at the 0.05 level.

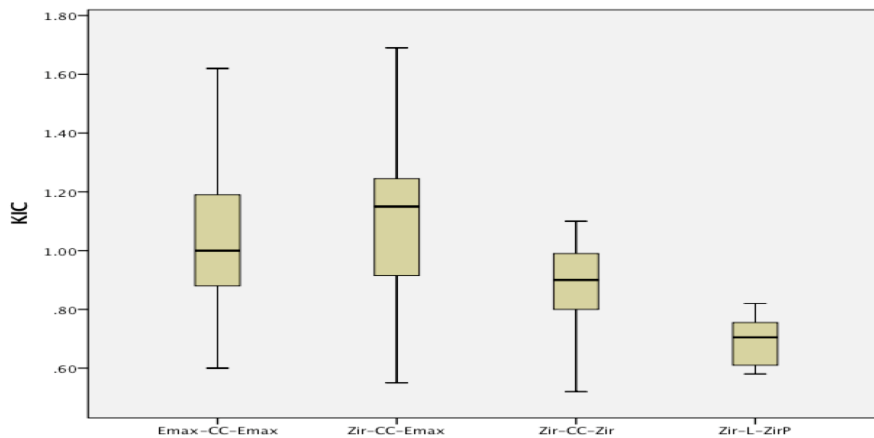
**Table 9: Scheffe multiple comparison test**

Figure 29 (p.59) shows Weibull plots of the results. The slope,  $m$ , represented by the dotted lines, provides a visual representation of the reliability for each of the tested groups. Higher  $m$  values, shown as steeper lines, represent a narrower range of values within which the test subjects fractured. As seen on the graph and confirmed in Table 9, the control group had the highest degree of reliability with an  $m$  value of 10.45. Groups I, II, and III had much lower reliability. Group I had an  $m$  value of 4.51, group II had an  $m$  value of 5.16, and group III a value of 4.34.



**Figure 29: Graphical representation of Weibull analysis results**

Figure 30 represents box plots of the interfacial  $K_{IC}$  for the tested groups. The box plot analysis clearly shows that the groups fused with CC have wider distributions and higher interfacial  $K_{IC}$  values than the ZirPress control group.



**Figure 30: Box of the comparing interfacial  $K_{IC}$  and test groups SEM analysis**

## 5.2. Scanning Electron Microscopy

In order to characterize the surface of the materials prior to bonding, several unfractured and untested half prism samples were scanned. The scans of the untested half prism would enable a comparison with tested fractured samples. Figures 31 and 32 (pp.60-61) are SEM micrograph images of unfused and Y-TZP and LS2 half prism samples. The samples have numerous parallel striations on the pre-fused test surfaces. The SEM images revealed that all the non-bonded half samples had similar striations. The grooves on the unfused sides are thought to have been produced by the Isomet diamond cutting disks during sectioning of the prisms. Although the surfaces appear to be rough due to the diamond-cutting blade, they are uniform in appearance and contain very few observable intrinsic defects.

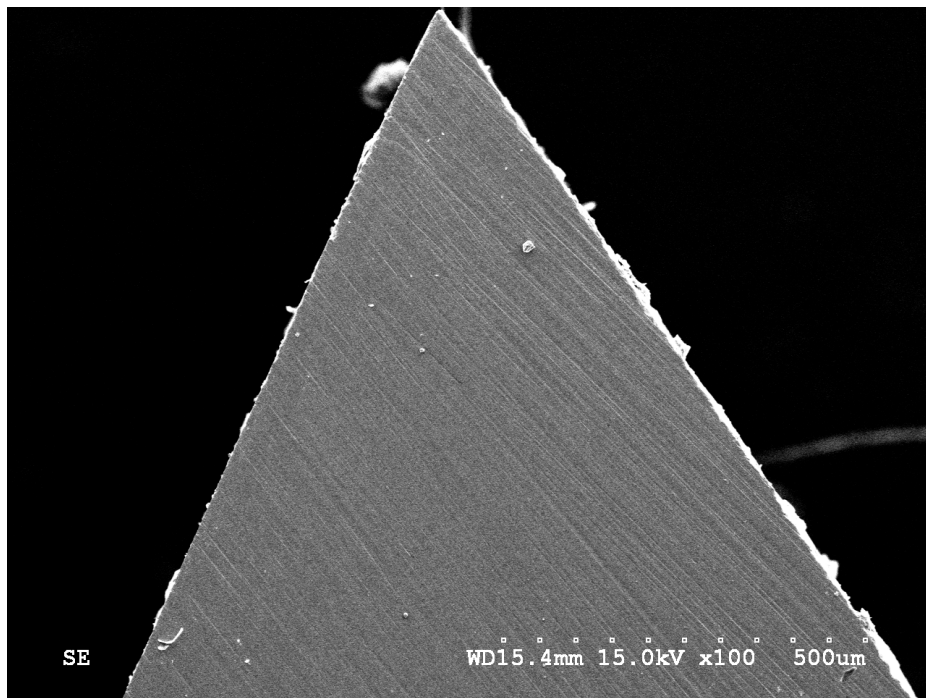


**Figure 31: IPS e.max ZirCAD NTP test half sample prior to glass fusion**

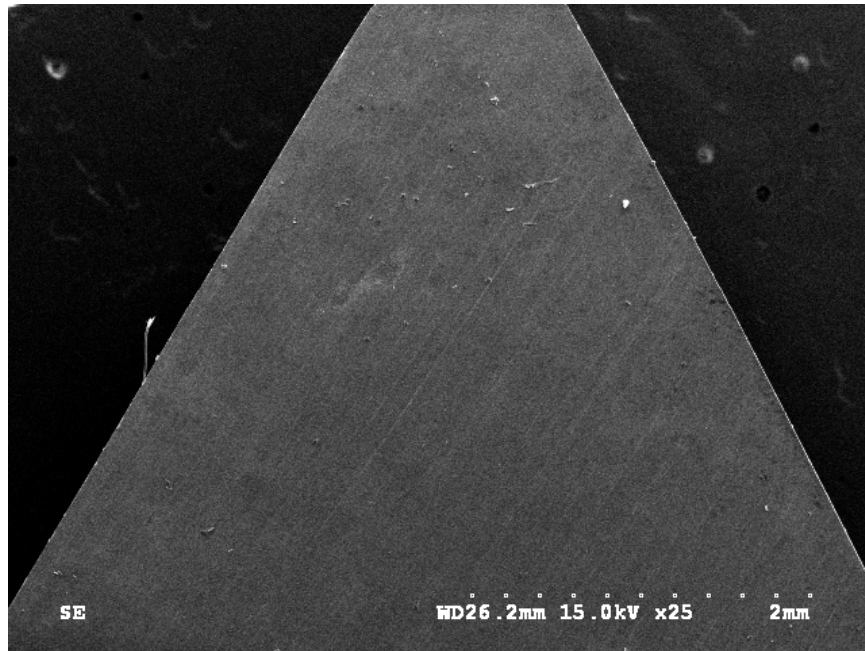
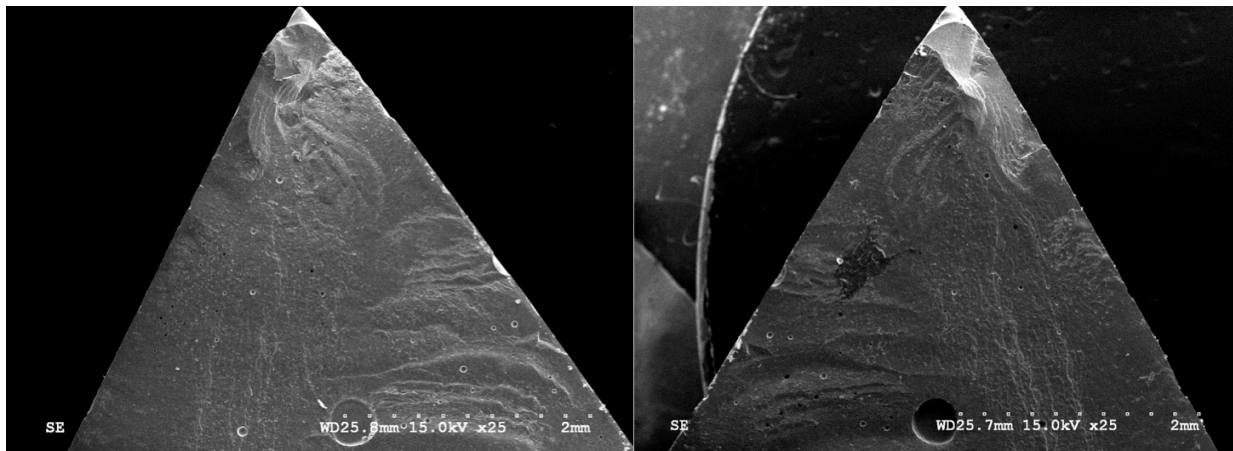


**Figure 32: IPS e.max CAD NTP test half sample prior to glass fusion**

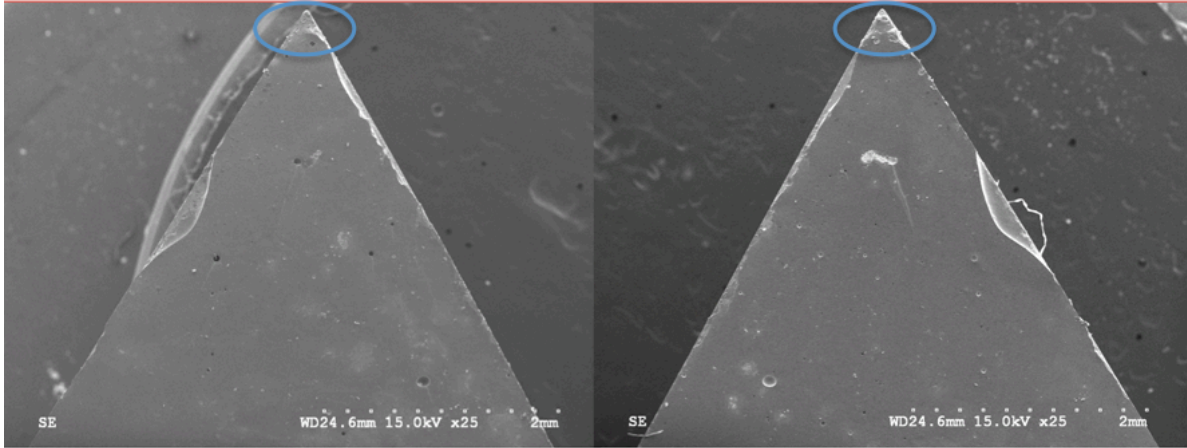
Figure 33 (p.62) shows two sides of a group I fractured test sample. These images are representative of the group and confirm the observations made under light microscope. These surfaces do not possess cutting wheel striations. The fracture surfaces also appeared to have an increased number of overall defects. Most the defects appear to be superficial and limited to the outer edges of the CC layer, potentially due to gas egress during the fusion step. These images confirm the light microscope observations of cohesive failure with glass residue on the LS2 bonding surface and crack propagating within the CC bonding layer. Similar behaviour was seen in most group I SEM images. The number of defects appears to be comparable to those seen in the other test groups.

Figure 34 (p.63) is a SEM image of two sides of a single fractured group II sample. The crack initiation area is highlighted in each image by blue circles. Unlike Figures 31 & 32 (pp.60-61),

these images do not have striations. All the remaining SEM images of group II half samples appeared to have fusing CC glass on both interface surfaces of the sample. It appears that there are numerous small defects in the glass. Some of these defects appear to pass through the glass fusion layer and terminate on the LS2 interface while others are superficial and appear to be limited to the CC layer. Defects positioned toward the centre of the sample are more spherical in nature, possibly representing gas trapped inside the CC during the fusion process. Defects that are closer to the edges of the samples appear to be more irregular in shape. Figure 33 coincides with most of the visual inspections performed under light microscope on fractured group II samples. During these inspections, these interfaces were described as possessing fusion glass on the fractured Y-TZP half samples. Although most of the fractured surfaces were smooth in appearance, some of the light microscope inspections revealed irregular distributions of the CC layer on the interfaces. Evidence from both the visual inspection and SEM images suggest that the crack propagated exclusively within the connecting glass.



**Figure 33: Two corresponding IPS e.max CAD NTP test half samples after fracture**



**Figure 34: Two corresponding IPS e.max ZirCAD NTP test half samples after fracture**

Figure 35 (p.64) shows a group III sample after glass fusion and fracture. This figure contains two sides of a fractured “CAD-on” sample, a LS<sub>2</sub> half sample and a Y-TZP half sample. As with the previous images, the micrographs are representative of the remainder of the “CAD-on” group and coincide with most of the observations made under light microscope. Unlike group I, the “CAD-on” samples fractured smoothly through the CC and appeared similar to group II fracture samples. Although a mixture of defects is present, their appearance was comparable to those observed in group II. Again, these images confirm the light microscope observations of cohesive failure within the “CAD-on” group with glass residue remaining equally on the LS<sub>2</sub> bonding surface and the Y-TZP surface with crack propagation occurring within the CC layer.

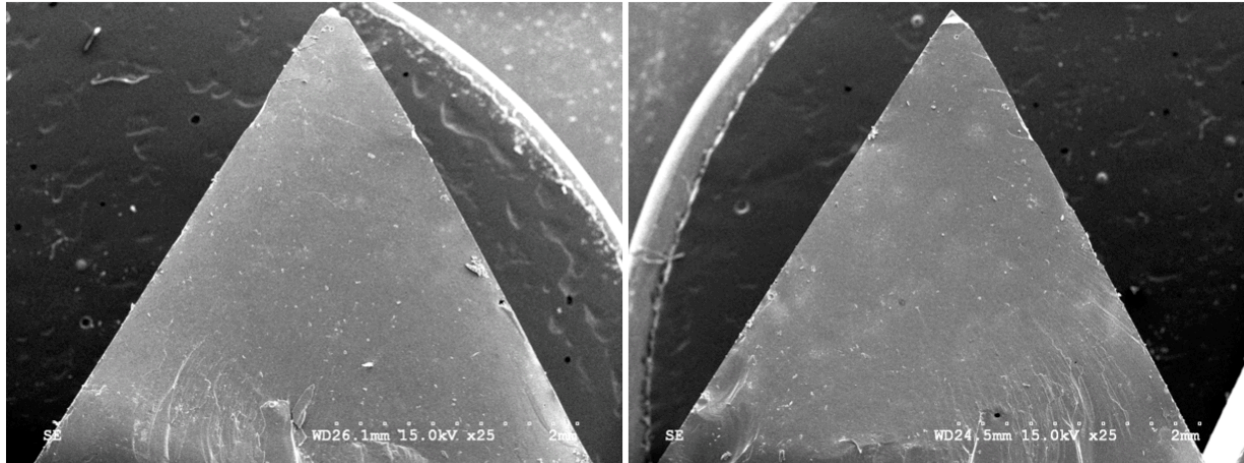


**Figure 35: ZirCAD e.max CAD (“CAD-on”) complex fracture sample**

Figure 35 shows two sides of a ZirPress control sample. Like the test samples, there is an obvious lack of striations on the surface of the zirconia half sample. Just as in Figures 32- 34 (pp.61-63), it appears that the ZirPress samples did not undergo adhesive failure between the zirconia half sample and the remainder of the triangular prism. Determining if the fractured halves underwent cohesive failure through the ZirLiner layer, or if the fracture traveled through the Zirpress portion of the sample is not possible because of the lack of a definitive junction on the ZirPress side of the sample. Unlike the test groups which possessed numerous large defects within the interface, qualitative light microscope and SEM observations of the control group revealed considerably fewer defects in the fracture surfaces. Defects seen in the control group were smaller in size and more irregular in shape than those in the test groups. Also, fractured surfaces in the control group were rougher, irregular, and had steps or ledges within the surface towards the edge of the sample. Unlike the test groups, the control group does not have easily identifiable striations on each of the half samples. The lack of striations on the ZirPress / Zirliner interface makes identifying the mode and location of failure difficult. However, the absence of striations on the ZirCAD portion of the

control group would exclude the possibility of an adhesive failure between the ZirCAD and ZirLiner interface.

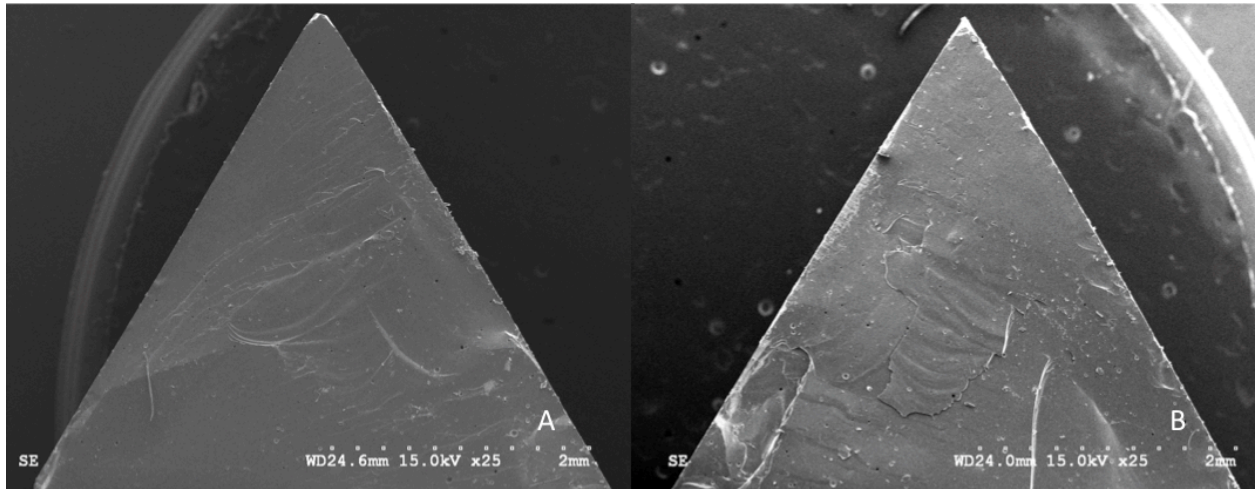


**Figure 36: IPS e.max ZirCAD with ZirPress (control)**

## Chapter 6: Discussion

Some interesting outcomes of this investigation include the differences in the observed characteristics of the fracture interfaces, cohesive failure within fusing glass of the test samples, lower test group Weibull moduli, and higher test group interfacial  $K_{IC}$  values.

Most of the test samples involving both the LS2 and Y-TZP interfaces appear to have undergone cohesive failure within the connecting glass. There did not appear to be a significant difference between the interfacial  $K_{IC}$  values interfaces involved in groups I and II. The lack of a significant difference meant that  $H_{01}$  was accepted. This result would imply that the “CAD-on” interface is limited primarily by the  $K_{IC}$  of the fusing glass. The Weibull characteristic  $K_{IC}$  values for the three test groups were not significantly different and ranged between  $0.92 \text{ MPa}\cdot\text{m}^{1/2}$  and  $1.24 \text{ MPa}\cdot\text{m}^{1/2}$ . Although the CC glass was not tested directly, it would not be unreasonable to conclude that the  $K_{IC}$  of the CC likely lies close to the range or the test group  $K_{IC}$  values.

The reliability of the “CAD-on” complex was found to be significantly lower than the pressed veneer control group. Initially, this result may seem unexpected since commercially produced ceramics, such as an e.max CAD ingot, are thought to be more reliable due to fewer internal flaws. However, this investigation did not examine the strength of the CAD/CAM veneers, but instead examined the  $K_{IC}$  of the adhesive interfaces between the veneers. The adhesive interface of the control group was obtained via hot pressing. The adhesive interfaces involved in the test groups were obtained via manipulation of a thixotropic slurry of glass. Maintaining control over the degree of vibration, the consistency of the glass, and the amount of air incorporated into the slurry was difficult. It would be reasonable to assume that an interface produced from the vibrated glass slurry

would be less consistent, incorporate more defects, and be less reliable than a pneumatically pressed interface.

The lower reliability computed for the three test groups may be attributable to defects within the glass fusion layer. Examination of the test specimens under both light microscope and SEM (Figures 31 – 34, pp.60-63), revealed many circular porosities/voids within the fractured interfaces of the connecting glass. The size, number, and distribution of the defects within the fusion layer or the veneering layer would be important contributing factors to the difference between the reliabilities of the control and test groups. The Weibull modulus, which indicates reliability, was calculated to be 10.45 for the control. The calculated Weibull moduli for the test groups ranged between 4 and 5. The significantly higher value for the control group confirms that the control group is more reliable and corresponds with the larger distribution, number, and size of flaws present in the test groups. While the CC test groups contained round flaws that would suggest the presence of gasses during the fusion stage, the control group appeared to have fewer porosities or incorporated defects. Contrasting the test samples, the ZirPress fractures also appeared to have smaller flaws and a smoother fracture surface. Of note, since the fractures were occurring within the glass fusion layer, the theorized superior consistency of the commercial veneering ceramic does not appear have contributed to the interfacial  $K_{IC}$  of the test groups.

It is well recognized that the strength of the bond between the veneering ceramic and zirconia can be influenced by differences between coefficients of thermal expansion. Stresses related to thermal mismatch within veneered all ceramic restorations will affect crack propagation. Under the plane strain conditions of Equation 4B (p.27), the energy required for a defect to undergo crack

propagation can be increased or decreased depending on the type of strain present in the surrounding ceramic material. For defects under tensile strain, less external energy is required to initiate crack propagation, and the  $K_{IC}$  of the material is lowered. Veneering ceramics that more closely match one another's thermal properties have less residual internal stress and are more likely to exhibit higher and more uniform  $K_{IC}$  values. In this case, ZirCAD, ZirLiner, and ZirPress have CTEs of 10.50 ppm /K, 9.90 ppm /K and 9.85 ppm /K respectively, while IPS e.max and CC have CTEs of 10.20 ppm /K and 9.50 ppm /K respectively. The similar CTEs of the control group, and the added complex stresses of additional glass layers in the test groups, may have produced more internal strain throughout the test group samples. If so, the strain may have reduced the consistency of interfacial  $K_{IC}$  values and contributed to the lower Weibull moduli within the test groups.

The method of producing the test samples may also have contributed to the incorporation of errors in the fusion glass. During approximation of the two half specimens, the half sections and the connecting glass were vibrated in order to cause the thixotropic CC to undergo liquefaction and settle between the two half prisms. It would be reasonable to assume that voids and air could become incorporated and trapped within the glass fusion substrate. The incorporation of voids into the test samples during production could explain the significant difference between the test and control group Weibull moduli.

Although initially intended for tooth-supported restorations, the "CAD-on" technique may also have future with implant-supported restorations. Currently, there are few aesthetic translucent all ceramic restorations capable of withstanding the masticatory forces in the posterior regions of the mouth. Some of the available choices include monolithic ceramic materials that do not possess

veneering structures, such as single unit LS2 or multi-unit zirconia restorations. Other types consist of high-strength ceramic frameworks pressed or hand sintered with more esthetic feldspathic-based porcelains. Conventional MCC veneered with feldspathic porcelain are also still in use. The clinical use of zirconia-based restorations are increasing because of its strength, ease of fabrication, dimensional stability, and its higher  $K_{IC}$ . As stated previously, one of the weak points of a zirconia restoration is the cracking or failure of its veneer. Consequently, the ability to produce an aesthetic zirconia restoration with a veneer with an improved ability to resist fracture is meaningful. Although glass-fused restorations appear to possess more defects and are less reliable than conventional zirconia veneering, all but the weakest of “CAD-on” samples matched or exceeded the majority of conventional controls. Slight improvements in processing, or an alternative method of application could result in a significant gain over conventional veneering by “CAD-on”. These positive results combined with an improvement in production efficiency could result in the “CAD-on” technique having significant clinical implications.

## Chapter 7: Conclusions

Based on the results of this study, the “CAD-on” technique resulted in crowns that may be more resistant to fracture compared to conventional veneered crowns. The statistical analysis demonstrated that there was no significant difference between the  $K_{IC}$  values of the two interfaces present in “CAD-on” crowns. The results suggested that the interfacial  $K_{IC}$  present in “CAD-on” crowns is limited by the  $K_{IC}$  of the connecting glass. These results also suggested that “CAD-on” crowns have a higher  $K_{IC}$  than conventional ZirPress veneered crowns and may therefore perform better in posterior application. Results of long-term clinical trials are needed to confirm these results.

## References

- [1] Zarone F, Russo S, Sorrentino R. From porcelain-fused-to-metal to zirconia: clinical and experimental considerations. *Dent Mater.* 2011;27:83-96.
- [2] Behr M, Zeman F, Baitinger T, Galler J, Koller M, Handel G et al. The clinical performance of porcelain-fused-to-metal precious alloy single crowns: chipping, recurrent caries, periodontitis, and loss of retention. *Int J Prosthodont.* 2014;27:153-60.
- [3] Tysowsky GW. The science behind lithium disilicate: a metal-free alternative. *Dent Today.* 2009;28:112-3.
- [4] Della Bona A, Kelly JR. The clinical success of all-ceramic restorations. *J Am Dent Assoc.* 2008;139 Suppl:8s-13s.
- [5] Chaar MS, Witkowski S, Strub JR, Att W. Effect of veneering technique on the fracture resistance of zirconia fixed dental prostheses. *J Oral Rehabil.* 2013;40:51-9.
- [6] Sravanthi Y, Ramani YV, Rathod AM, Ram SM, Turakhia H. The comparative evaluation of the translucency of crowns fabricated with three different all-ceramic materials: an in vitro study. *J Clin Diagn Res.* 2015;9:Zc30-4.
- [7] Guess PC, Schultheis S, Bonfante EA, Coelho PG, Ferencz JL, Silva NR. All-ceramic systems: laboratory and clinical performance. *Dent Clin North Am.* 2011;55:333-52, ix.
- [8] Marquardt P, Strub JR. Survival rates of IPS empress 2 all-ceramic crowns and fixed partial dentures: results of a 5-year prospective clinical study. *Quintessence Int.* 2006;37:253-9.
- [9] Pieger S, Salman A, Bidra AS. Clinical outcomes of lithium disilicate single crowns and partial fixed dental prostheses: a systematic review. *J Prosthet Dent.* 2014;112:22-30.
- [10] Rues S, Kroger E, Muller D, Schmitter M. Effect of firing protocols on cohesive failure of all-ceramic crowns. *J Dent.* 2010;38:987-94.

- [11] Rezaei SM, Heidarifar H, Arezodar FF, Azary A, Mokhtarykhomee S. Influence of Connector Width on the Stress Distribution of Posterior Bridges under Loading. *J Dent (Tehran)*. 2011;8:67-74.
- [12] Renda JJ, Harding AB, Bailey CW, Guillory VL, Vandewalle KS. Microtensile bond strength of lithium disilicate to zirconia with the CAD-on technique. *J Prosthodont*. 2015;24:188-93.
- [13] Agustin-Panadero R, Roman-Rodriguez JL, Ferreiroa A, Sola-Ruiz MF, Fons-Font A. Zirconia in fixed prosthesis. A literature review. *J Clin Exp Dent*. 2014;6:e66-73.
- [14] Koutayas SO, Vagkopoulou T, Pelekanos S, Koidis P, Strub JR. Zirconia in dentistry: part 2. Evidence-based clinical breakthrough. *Eur J Esthet Dent*. 2009;4:348-80.
- [15] Rekow ED, Silva NR, Coelho PG, Zhang Y, Guess P, Thompson VP. Performance of dental ceramics: challenges for improvements. *J Dent Res*. 2011;90:937-52.
- [16] Gautam C, Joyner J, Gautam A, Rao J, Vajtai R. Zirconia based dental ceramics: structure, mechanical properties, biocompatibility and applications. *Dalton Trans*. 2016.
- [17] Triwatana P, Nagaviroj N, Tulapornchai C. Clinical performance and failures of zirconia-based fixed partial dentures: a review literature. *J Adv Prosthodont*. 2012;4:76-83.
- [18] Al-Amleh B, Lyons K, Swain M. Clinical trials in zirconia: a systematic review. *J Oral Rehabil*. 2010;37:641-52.
- [19] Miyazaki T, Nakamura T, Matsumura H, Ban S, Kobayashi T. Current status of zirconia restoration. *J Prosthodont Res*. 2013;57:236-61.
- [20] Chrcanovic BR, Abreu MH. Survival and complications of zygomatic implants: a systematic review. *Oral Maxillofac Surg*. 2013;17:81-93.

- [21] Schley JS, Heussen N, Reich S, Fischer J, Haselhuhn K, Wolfart S. Survival probability of zirconia-based fixed dental prostheses up to 5 yr: a systematic review of the literature. *Eur J Oral Sci.* 2010;118:443-50.
- [22] Ivoclarvivadent. Scientific Documentation IPS e.max® CAD-on Schaan (LI): Ivoclarvivadent; 2011 [cited Aug 10th 2016. Available from: <http://www.ivoclarvivadent.com/zoolu-website/media/document/12250/IPS+e-max+CAD-on>.
- [23] Guess PC, Zavanelli RA, Silva NR, Bonfante EA, Coelho PG, Thompson VP. Monolithic CAD/CAM lithium disilicate versus veneered Y-TZP crowns: comparison of failure modes and reliability after fatigue. *Int J Prosthodont.* 2010;23:434-42.
- [24] Tinschert J, Zvez D, Marx R, Anusavice KJ. Structural reliability of alumina-, feldspar-, leucite-, mica- and zirconia-based ceramics. *J Dent.* 2000;28:529-35.
- [25] Smith WF. Principles of materials science and engineering. 1986.
- [26] Anusavice KJ, Shen C, Rawls HR. Phillips' science of dental materials: Elsevier Health Sciences; 2013.
- [27] Zumdahl S. Zumdahl Chemistry. Houghton Mifflin, New York; 1997.
- [28] Powers JM, Craig RG. Restorative dental materials, 11/e: Elsevier India; 2002.
- [29] Hume N. *Ivor. A Guide to Artifacts of Colonial America.* New York: Alfred A Knopf; 1980.
- [30] Henderson J. The science and archaeology of materials: an investigation of inorganic materials: Routledge; 2013.
- [31] Sakaguchi RL, Powers JM. Craig's restorative dental materials: Elsevier Health Sciences; 2012.
- [32] is U. Effect of Veneering Techniques on Ceramic Fracture of Zirconia Restoration. Unknown

- [33] Helvey G. Ceramics. *Compend Contin Educ Dent*. 2010;31:309-11.
- [34] Kelly JR, Nishimura I, Campbell SD. Ceramics in dentistry: historical roots and current perspectives. *J Prosthet Dent*. 1996;75:18-32.
- [35] Barreiro MM, Riesgo O, Vicente EE. Phase identification in dental porcelains for ceramometallic restorations. *Dent Mater*. 1989;5:51-7.
- [36] Mackert JR, Jr., Butts MB, Fairhurst CW. The effect of the leucite transformation on dental porcelain expansion. *Dent Mater*. 1986;2:32-6.
- [37] Le M, Papia E, Larsson C. The clinical success of tooth- and implant-supported zirconia-based fixed dental prostheses. A systematic review. *J Oral Rehabil*. 2015;42:467-80.
- [38] Sailer I, Makarov NA, Thoma DS, Zwahlen M, Pjetursson BE. All-ceramic or metal-ceramic tooth-supported fixed dental prostheses (FDPs)? A systematic review of the survival and complication rates. Part I: Single crowns (SCs). *Dent Mater*. 2015;31:603-23.
- [39] Swain MV. Unstable cracking (chipping) of veneering porcelain on all-ceramic dental crowns and fixed partial dentures. *Acta Biomater*. 2009;5:1668-77.
- [40] Pjetursson BE, Sailer I, Zwahlen M, Hammerle CH. A systematic review of the survival and complication rates of all-ceramic and metal-ceramic reconstructions after an observation period of at least 3 years. Part I: Single crowns. *Clin Oral Implants Res*. 2007;18 Suppl 3:73-85.
- [41] Shenoy A, Shenoy N. Dental ceramics: An update. *J Conserv Dent*. 2010;13:195-203.
- [42] Smith WF, Hashemi J. *Foundations of materials science and engineering*: McGraw-Hill; 2011.
- [43] Ivoclarvivadent. IPS e.max® – one system for every indication Schaan (LI): Ivoclarvivadent; 2008 [cited Jan 6<sup>th</sup> 2016. Available from: <http://biocaddental.ca/wp-content/uploads/2011/09/IPS+e-max+System+Dentist2.pdf>.

- [44] Kang SH, Chang J, Son HH. Flexural strength and microstructure of two lithium disilicate glass ceramics for CAD/CAM restoration in the dental clinic. *Restor Dent Endod.* 2013;38:134-40.
- [45] Wolfram H, Beall G. *Glass-ceramic technology*: American Ceramic Society; 2002.
- [46] Alkadi L, Ruse ND. Fracture toughness of two lithium disilicate dental glass ceramics. *J Prosthet Dent.* 2016.
- [47] Thornton I. *Mechanical properties of dental resin composite CAD/CAM blocks*: University of British Columbia; 2014.
- [48] Ivoclarvivadent. *IPS e.max Press Scientific Documentation*. Schaan (LI): Ivoclarvivadent; 2007 [Cited August 14<sup>th</sup> 2016]. Available from: <https://www.ivoclarvivadent.com/zoolu-website/media/document/10473/IPS+e-max+ZirPress>.
- [49] Cortellini D, Canale A. Bonding lithium disilicate ceramic to feather-edge tooth preparations: a minimally invasive treatment concept. *J Adhes Dent.* 2012;14:7-10.
- [50] Fabbri G, Zarone F, Dellificorelli G, Cannistraro G, De Lorenzi M, Mosca A et al. Clinical evaluation of 860 anterior and posterior lithium disilicate restorations: retrospective study with a mean follow-up of 3 years and a maximum observational period of 6 years. *Int J Periodontics Restorative Dent.* 2014;34:165-77.
- [51] Valenti M, Valenti A. Retrospective survival analysis of 261 lithium disilicate crowns in a private general practice. *Quintessence Int.* 2009;40:573-9.
- [52] Toman M, Toksavul S. Clinical evaluation of 121 lithium disilicate all-ceramic crowns up to 9 years. *Quintessence Int.* 2015;46:189-97.
- [53] Wolfart S, Eschbach S, Scherrer S, Kern M. Clinical outcome of three-unit lithium-disilicate glass-ceramic fixed dental prostheses: up to 8 years results. *Dent Mater.* 2009;25:e63-71.

- [54] Sola-Ruiz MF, Lagos-Flores E, Roman-Rodriguez JL, Highsmith Jdel R, Fons-Font A, Granell-Ruiz M. Survival rates of a lithium disilicate-based core ceramic for three-unit esthetic fixed partial dentures: a 10-year prospective study. *Int J Prosthodont.* 2013;26:175-80.
- [55] Lin WS, Ercoli C, Feng C, Morton D. The effect of core material, veneering porcelain, and fabrication technique on the biaxial flexural strength and weibull analysis of selected dental ceramics. *J Prosthodont.* 2012;21:353-62.
- [56] Soderholm KJ. Review of the fracture toughness approach. *Dent Mater.* 2010;26:e63-77.
- [57] Sailer I, Pjetursson BE, Zwahlen M, Hammerle CH. A systematic review of the survival and complication rates of all-ceramic and metal-ceramic reconstructions after an observation period of at least 3 years. Part II: Fixed dental prostheses. *Clin Oral Implants Res.* 2007;18 Suppl 3:86-96.
- [58] Olsson KG, Furst B, Andersson B, Carlsson GE. A long-term retrospective and clinical follow-up study of In-Ceram Alumina FPDs. *Int J Prosthodont.* 2003;16:150-6.
- [59] Denry IL. Recent advances in ceramics for dentistry. *Crit Rev Oral Biol Med.* 1996;7:134-43.
- [60] Conrad HJ, Seong W-J, Pesun IJ. Current ceramic materials and systems with clinical recommendations: a systematic review. *J Prosthet Dent.* 2007;98:389-404.
- [61] Guazzato M, Albakry M, Ringer SP, Swain MV. Strength, fracture toughness and microstructure of a selection of all-ceramic materials. Part I. Pressable and alumina glass-infiltrated ceramics. *Dent Mater.* 2004;20:441-8.
- [62] Wassermann A, Kaiser M, Strub JR. Clinical long-term results of VITA In-Ceram Classic crowns and fixed partial dentures: A systematic literature review. *Int J Prosthodont.* 2006;19:355-63.

- [63] Guazzato M, Albakry M, Ringer SP, Swain MV. Strength, fracture toughness and microstructure of a selection of all-ceramic materials. Part II. Zirconia-based dental ceramics. *Dent Mater.* 2004;20:449-56.
- [64] Chaar MS, Passia N, Kern M. Ten-year clinical outcome of three-unit posterior FDPs made from a glass-infiltrated zirconia reinforced alumina ceramic (In-Ceram Zirconia). *J Dent.* 2015;43:512-7.
- [65] Christensen JJ. Achieving optimal outcomes with all-zirconia crowns. *Gen Dent.* 2014;62:e6-9.
- [66] Blatz MB, Alvarez M, Sawyer K, Brindis M. How to Bond Zirconia: The APC Concept. *Compend Contin Educ Dent.* 2016;37:611-7; quiz 8.
- [67] Raigrodski AJ, Hillstead MB, Meng GK, Chung KH. Survival and complications of zirconia-based fixed dental prostheses: a systematic review. *J Prosthet Dent.* 2012;107:170-7.
- [68] Guess PC, Zhang Y, Thompson VP. Effect of veneering techniques on damage and reliability of Y-TZP trilayers. *Eur J Esthet Dent.* 2009;4:262-76.
- [69] Combe EC, Burke FT, Douglas WH. *Dental biomaterials*: Kluwer Academic Publishers; 1999.
- [70] Ramos CM, Cesar PF, Bonfante EA, Rubo JH, Wang L, Borges AF. Fractographic principles applied to Y-TZP mechanical behavior analysis. *J Mech Behav Biomed Mater.* 2016;57:215-23.
- [71] Homaei E, Farhangdoost K, Tsoi JK, Matinlinna JP, Pow EH. Static and fatigue mechanical behavior of three dental CAD/CAM ceramics. *J Mech Behav Biomed Mater.* 2016;59:304-13.
- [72] Seghi RR, Denry IL, Rosenstiel SF. Relative fracture toughness and hardness of new dental ceramics. *J Prosthet Dent.* 1995;74:145-50.

- [73] Subash M, Vijitha D, Deb S, Satish A, Mahendirakumar N. Evaluation of shear bond strength between zirconia core and ceramic veneers fabricated by pressing and layering techniques: In vitro study. *J Pharm Bioallied Sci.* 2015;7:S612-5.
- [74] Ivoclarvivadent. IPS e.amx ZirPress Scientific Documentation. Schaan (LI): Ivoclarvivadent; 2007 [Cited July 6<sup>th</sup> 2016]. Available from: <https://www.ivoclarvivadent.com/zoolu-website/media/document/10473/IPS+e-max+ZirPress>.
- [75] Augstin-Panadero R, Fons-Font A, Roman-Rodriguez JL, Granell-Ruiz M, del Rio-Highsmith J, Sola-Ruiz MF. Zirconia versus metal: a preliminary comparative analysis of ceramic veneer behavior. *Int J Prosthodont.* 2012;25:294-300.
- [76] Lopez-Molla MV, Martinez-Gonzalez MA, Manes-Ferrer JF, Amigo-Borras V, Bouazza-Juanes K. Bond strength evaluation of the veneering-core ceramics bonds. *Med Oral Patol Oral Cir Bucal.* 2010;15:e919-23.
- [77] Lopez-Molla MV, Martinez-Gonzalez A, Amigo-Borras V, Manes-Ferrer JF. Fractographic Study of the Interface Between Zirconia Y-TZP and Its Veneering Ceramic After Shear Strength Testing. *Int J Prosthodont.* 2015;28:432-4.
- [78] Stawarczyk B, Ozcan M, Roos M, Trottmann A, Sailer I, Hammerle CH. Load-bearing capacity and failure types of anterior zirconia crowns veneered with overpressing and layering techniques. *Dent Mater.* 2011;27:1045-53.
- [79] Choi JE, Waddell JN, Torr B, Swain MV. Pressed ceramics onto zirconia. Part 1: Comparison of crystalline phases present, adhesion to a zirconia system and flexural strength. *Dent Mater.* 2011;27:1204-12.
- [80] Beuer F, Stimmelmayer M, Gernet W, Edelhoff D, Guh JF, Naumann M. Prospective study of zirconia-based restorations: 3-year clinical results. *Quintessence Int.* 2010;41:631-7.

- [81] Yoon HI, Yeo IS, Yi YJ, Kim SH, Lee JB, Han JS. Effect of various intermediate ceramic layers on the interfacial stability of zirconia core and veneering ceramics. *Acta Odontol Scand.* 2015;73:488-95.
- [82] Koenig V, Vanheusden AJ, Le Goff SO, Mainjot AK. Clinical risk factors related to failures with zirconia-based restorations: an up to 9-year retrospective study. *J Dent.* 2013;41:1164-74.
- [83] Aboushelib MN, Feilzer AJ, Kleverlaan CJ. Bridging the gap between clinical failure and laboratory fracture strength tests using a fractographic approach. *Dent Mater.* 2009;25:383-91.
- [84] Kanat-Erturk B, Comlekoglu EM, Dundar-Comlekoglu M, Ozcan M, Gungor MA. Effect of Veneering Methods on Zirconia Framework-Veneer Ceramic Adhesion and Fracture Resistance of Single Crowns. *J Prosthodont.* 2015;24:620-8.
- [85] Tzanakakis EG, Tzoutzas IG, Koidis PT. Is there a potential for durable adhesion to zirconia restorations? A systematic review. *J Prosthet Dent.* 2016;115:9-19.
- [86] Stutes RD. The history and clinical application of a chairside CAD/CAM dental restoration system. *Shanghai kou qiang yi xue= Shanghai journal of stomatology.* 2006;15:449-55.
- [87] Kaur I, Datta K. CEREC-The power of technology. *J Ind Prosthodont Soc.* 2006;6:115.
- [88] Miyazaki T, Hotta Y, Kunii J, Kuriyama S, Tamaki Y. A review of dental CAD/CAM: current status and future perspectives from 20 years of experience. *Dent Mater J.* 2009;28:44-56.
- [89] Masri R, Driscoll C. *Clinical Applications of Digital Dental Technology*; John Wiley & Sons; 2015.
- [90] Spiegel TAM. *The CAD-on technique*. 1 ed: DGI Dental Publishing; 2012.
- [91] Alghazzawi TF. Advancements in CAD/CAM technology: Options for practical implementation. *J Prosthodont Res.* 2016;60:72-84.

- [92] Beuer F, Schweiger J, Eichberger M, Kappert HF, Gernet W, Edelhoff D. High-strength CAD/CAM-fabricated veneering material sintered to zirconia copings--a new fabrication mode for all-ceramic restorations. *Dent Mater.* 2009;25:121-8.
- [93] Schmitter M, Mueller D, Rues S. Chipping behaviour of all-ceramic crowns with zirconia framework and CAD/CAM manufactured veneer. *J Dent.* 2012;40:154-62.
- [94] Basso GR, Moraes RR, Borba M, Griggs JA, Della Bona A. Flexural strength and reliability of monolithic and trilayer ceramic structures obtained by the CAD-on technique. *Dent Mater.* 2015;31:1453-9.
- [95] Basso GR, Moraes RR, Borba M, Duan Y, Griggs JA, Bona AD. Reliability and failure behavior of CAD-on fixed partial dentures. *Dent Mater.* 2016;32:624-30.
- [96] Nossair SA, Aboushelib MN, Morsi TS. Fracture and Fatigue Resistance of Cemented versus Fused CAD-on Veneers over Customized Zirconia Implant Abutments. *J Prosthodont.* 2015;24:543-48.
- [97] Al-Dohan HM, Yaman P, Dennison JB, Razzoog ME, Lang BR. Shear strength of core-veneer interface in bi-layered ceramics. *J Prosthet Dent.* 2004;91:349-55.
- [98] Aboushelib MN, de Jager N, Kleverlaan CJ, Feilzer AJ. Microtensile bond strength of different components of core veneered all-ceramic restorations. *Dent Mater.* 2005;21:984-91.
- [99] Scherrer SS, Cesar PF, Swain MV. Direct comparison of the bond strength results of the different test methods: a critical literature review. *Dent Mater.* 2010;26:e78-93.
- [100] Sirisha K, Rambabu T, Shankar YR, Ravikumar P. Validity of bond strength tests: A critical review: Part I. *J Conserv Dent.* 2014;17:305-11.
- [101] Sano H, Kanemura N, Burrow MF, Inai N, Yamada T, Tagami J. Effect of operator variability on dentin adhesion: students vs. dentists. *Dent Mater J.* 1998;17:51-8.

- [102] Braga RR, Meira JB, Boaro LC, Xavier TA. Adhesion to tooth structure: a critical review of "macro" test methods. *Dent Mater.* 2010;26:e38-49.
- [103] Sirisha K, Rambabu T, Ravishankar Y, Ravikumar P. Validity of bond strength tests: A critical review-Part II. *J Conserv Dent.* 2014;17:420-6.
- [104] Hertzberg RW. *Deformation and fracture mechanics of engineering materials*: Wiley; 1996.
- [105] Ruse N. Fracture mechanics characterization of dental biomaterials. *Dental Biomaterials: Imaging, Testing and Modelling*: Woodhead Pub., Cambridge, UK; 2008. p. 261-93.
- [106] Wang H, Pallav P, Isgro G, Feilzer AJ. Fracture toughness comparison of three test methods with four dental porcelains. *Dent Mater.* 2007;23:905-10.
- [107] Fischer H, Marx R. Fracture toughness of dental ceramics: comparison of bending and indentation method. *Dent Mater.* 2002;18:12-9.
- [108] Baker A, Davis M, Hawkes G. Repair of fatigue cracked aircraft structures with advanced fibre composites: residual stress and thermal fatigue studies. *Proceedings of the 10th ICAF symposium in Brussels* Edited by Maenhaut, A, International Committee on Aeronautical Fatigue 1979. p. 4.3.
- [109] Ruse ND, Troczynski T, MacEntee MI, Feduik D. Novel fracture toughness test using a notchless triangular prism (NTP) specimen. *J Biomed Mater Res.* 1996;31:457-63.
- [110] Bubsey R, Munz D, Pierce W, Shannon Jr J. Compliance calibration of the short rod chevron-notch specimen for fracture toughness testing of brittle materials. *Int J Fract.* 1982;18:125-33.
- [111] Lawson NC, Bansal R, Burgess JO. Wear, strength, modulus and hardness of CAD/CAM restorative materials. *Dent Mater.* 2016.

- [112] Ivoclarvivadent. Scientific Documentation IPS e.max® ZirCAD [Scientific documentation]. Schaan (LI): Ivoclarvivadent; 2010 [Cited Mar 8<sup>th</sup> 2016]. Available from: <https://www.ivoclarvivadent.com/zoolu-website/media/document/1266/IPS+e-max+ZirCAD>.
- [113] Ivoclarvivadent. IPS e.amx Veneering Solutions Instructions for Use Schaan (LI): Ivoclarvivadent; 2014 [Cited Aug 03<sup>rd</sup> 2016]. Available from: <https://www.ivoclarvivadent.com/zoolu-website/media/document/7750/IPS+e-max+CAD+Veneering+Solution>.
- [114] Gehrt M, Wolfart S, Rafai N, Reich S, Edelhoff D. Clinical results of lithium-disilicate crowns after up to 9 years of service. *Clin Oral Investig*. 2013;17:275-84.
- [115] Christensen RP, Ploeger BJ. A clinical comparison of zirconia, metal and alumina fixed-prosthesis frameworks veneered with layered or pressed ceramic: a three-year report. *J Am Dent Assoc*. 2010;141:1317-29.
- [116] Fasbinder DJ, Dennison JB, Heys D, Neiva G. A clinical evaluation of chairside lithium disilicate CAD/CAM crowns: a two-year report. *J Am Dent Assoc*. 2010;141 Suppl 2:10s-4s.
- [117] Naenni N, Bindl A, Sax C, Hammerle C, Sailer I. A randomized controlled clinical trial of 3-unit posterior zirconia-ceramic fixed dental prostheses (FDP) with layered or pressed veneering ceramics: 3-year results. *J Dent*. 2015;43:1365-70.
- [118] Van Belle G. *Statistical rules of thumb*. Hoboken, NJ: Wiley; 2008.
- [119] Della Bona A, Mecholsky JJ, Jr., Anusavice KJ. Fracture behavior of lithia disilicate- and leucite-based ceramics. *Dent Mater*. 2004;20:956-62.
- [120] Quinn JB, Quinn GD, Sundar V. Fracture Toughness of Veneering Ceramics for Fused to Metal (PFM) and Zirconia Dental Restorative Materials. *J Res Natl Inst Stand Technol*. 2010;115:343-52.

[121] Ibrahim WM, McCabe JF. The use of Weibull statistics in mechanical testing of brittle dental materials. *J Nihon Univ School Dent.* 1993;35:225.

[122] Langlois R. Estimation of Weibull parameters. *J Mater Sci Let.* 1991;10:1049-51.

[123] Quinn JB, Quinn GD. A practical and systematic review of Weibull statistics for reporting strengths of dental materials. *Dent Mater.* 2010;26:135-47.